THESIS

REMOTE SENSING ASSESSMENTS OF CONSUMPTIVE USE OF AGRICULTURAL WATER IN WESTERN SLOPE OF COLORADO

Submitted by

Amandeep Vashisht

Department of Civil and Environmental Engineering

In partial fulfillment of the requirements

For the Degree of Master of Science

Colorado State University

Fort Collins, Colorado

Fall 2016

Master's Committee:

Advisor: José L. Chávez
Co-Advisor: Perry E. Cabot

Stephen J. Leisz

ABSTRACT

REMOTE SENSING ASSESSMENTS OF CONSUMPTIVE USE OF AGRICULTURAL WATER IN WESTERN SLOPE OF COLORADO

The Western Slope of Colorado is drained by Colorado River and its tributaries, which are facing increased pressure on their water resources due to prolonged droughts and increasing demands. While water is a limited resource, agriculture uses more than half of the total diverted water in the area. In such a scenario, agricultural water can be a likely supply for water conservation and sharing. The quantification of precise amount of water consumed by agricultural crops, or, consumptive use, is crucial for water sharing under temporary water sharing arrangements like water banks. Remote Sensing is considered as the most feasible method to determine spatial actual crop water use over large areas.

A preliminary performance evaluation of ReSET model for daily consumptive water use estimates under energy limiting and water limiting conditions was done. Conserved Consumptive Use estimates from plots replicating historical (full irrigation) and operational water bank (reduced irrigation) conditions were made on a monthly basis. In addition, crop growth stage information for grass and alfalfa pastures of the Western Slope was determined using Landsat and Sentinel satellites. An empirical relation between vegetation index (VI) and crop coefficient (Kc) was developed for use with reflectance-based crop coefficient approach. Lastly, reflectance-based approach for grass and alfalfa pastures was evaluated with ReSET-derived daily estimates of crop consumptive use.

ACKNOWLEDGEMENTS

I am thankful to my advisor, Dr. Jose Chavez for his support. I deeply appreciate all the guidance and advice provided by my co-advisor, Dr. Perry Cabot, who has been a mentor not only throughout this work, but in various aspects of professional life. My deepest gratitude to my committee member, Dr. Stephen Leisz for his thoughtful comments, and for letting me use his laboratory- without which this work would have not been possible. I am thankful to Dr. Aymn Elhaddad for providing me with the coded version of the model, which saved me a lot of time and trouble.

I extend my gratitude to my fellow graduate students and friends, Manijeh Mahmoudzadeh-Varzi, Mahmoud Soliman, and Emily Kullberg with whom I discussed and explored different ideas. I am thankful to Sumit Gautam and Carter Stoudt for field data collection.

This work was funded by Colorado Water Conservation Board, additional support provided by Colorado River District, The Nature Conservancy, Trout Unlimited and The No Chico Brush farmer-led focus group. I also appreciate the research work experience at NASA DEVELOP where I learned crucial remote sensing and geospatial skills. Lastly, I thank my parents and family for their moral support and encouragement every step of the way.

TABLE OF CONTENTS

LIST OF TABLES

LIST OF FIGURES

LIST OF SYMBOLS

ATM	Alternative Transfer Methods
CU	Consumptive Use
CCU	Conserved Consumptive Use
DEM	Digital Elevation Model
DP	Deep Percolation
ET	Evapotranspiration
ET_a	Actual Evapotranspiration
ET_{ref}	Reference evapotranspiration
ETrF	Evapotranspiration reference fraction
G	Ground heat flux
H	Sensible heat flux
I	Net Irrigation
Kc	Crop coefficient
Kcb	Basal crop coefficient
LAS	Large Aperture Scintillometer
LE	Latent heat flux
MAF	Million Acre Feet
NDVI	Normalized Difference Vegetation Index
NIR	Near Infra-Red
P	Effective Precipitation
R_n	Net Radiation
r_{ah}	Surface aerodynamic resistance to heat transfer
RH	Relative Humidity
SAVI	Soil Adjusted Vegetation Index
T_s	Surface radiometric temperature
TSM	Two Source Model

T_{aero}	Aerodynamic temperature
T_a	Air temperature
u	Wind speed
VI	Vegetation Index

CHAPTER 1: INTRODUCTION

Semi-arid climate of the Western US is characterized by low precipitation, making it highly vulnerable to effects of climate change-induced droughts. Non-climatic changes due to increasing human population growth are increasing pressure on limited water resources to fulfil demands for agriculture, urban landscape, municipality, industry, energy and, recreation sectors. Human activities are also responsible for deterioration of the quality of these limited water resources (Peters and Meybeck, 2007). At the same time, it is predicted that climate change would make precipitation more variable with the possibility of longer droughts (Barnett et al., 2008; Libecap, 2010). Other potential impacts of climate change could include increased frequency and magnitude of droughts and floods, and long-term changes in mean renewable water supplies through changes in precipitation, temperature, humidity, wind, duration of accumulated snowpack, nature and extent of vegetation, soil moisture, and runoff (Solomon et al., 2007).

Irrigated agriculture is the main user of diverted water globally, reaching a proportion that exceeds 70–80% of the total water diverted in the arid and semi-arid zones (Fereres and Soriano, 2007). In the United States, this sector consumes 65% of the water of all sectors (Hutson et al., 2004). In the western US, Colorado River is a water source for 4 upper basin states (Colorado, New Mexico, Utah and Wyoming), 3 lower basin states (Arizona, California and Nevada) in the US and Mexico. Roughly 90 percent of agricultural land in the Colorado River basin is irrigated, and 70 percent of the river's entire water supply is used for irrigation (Chen et al., 2015). The Colorado River Compact of 1922 regulates and ensures equitable distribution of water of

Colorado River. It requires the upper basin states to not to cause the flow, during any consecutive 10-year period, to fall below 9.25 billion cubic meters at Lee Ferry, the site that separates the upper and lower basin states. If the flow does fall below the specified amount for a consecutive 10-year period, curtailment of water in the upper basin is possible (Norviel et al., 1922).

In Colorado, the Western Slope is drained by the Colorado River and its tributaries. While about 80% of the water of Colorado is on the Western Slope, about 80% of the state population lives on the eastern Front Range. The senior water rights (the first to be fulfilled and reliable even in times of shortage) are largely held by agriculture, while Front Range cities have junior water rights and get from 30% to 50% of their water from the Western Slope in any given year (Best, 2009). Historical estimates of the Colorado River's base flow were determined to be approximately 18,500 million cubic meter per year (MacDonald, 2010). However, these estimates, which served as the basis for the river's allocations, were found to be optimistic, since they relied on historical flows based on records during a wet period. This has resulted in an over-allocated river system facing additional climate and population increase-related pressures (Chen et al., 2014).

A recent study on the Colorado River by Vano et al., 2014 projected a future streamflow decrease from 5% to 35% due to +2.5° ± 1°C warming in mid-twenty-first century. They estimated the ratio of annual runoff change to annual precipitation change (precipitation elasticity) at Lee Ferry to be between 2 and 3, as a result of which a 5% decline in precipitation will likely result in a 10%–15% decline in streamflow. The authors suggest substantial reductions in future Colorado River streamflow by the end of the twenty-first century due to a

combination of strong temperature-induced runoff curtailment and a probable reduction in annual precipitation. USBR (2012) projected the imbalance in supply and demand to be about 3.2 Million Acre Feet (MAF) by 2060. Such an imbalance could hinder water supply to junior water right holders, and could also potentially lead to a curtailment of water.

Agricultural water could be a likely supply for water conservation and sharing in such an environment. A more precise understanding is required of the quantities that can be conserved without jeopardizing the underlying agricultural and rural economies that depend on irrigated agriculture. In the Western US, water rights are distinct property rights not tied to the land, and water can be transferred among different users. "A water transfer is a voluntary agreement that results in a temporary or permanent change in the type, time, or place of use of water and/or a water right. Water transfers can be local or distant; they can be a sale, lease, or donation; and they can move water among agricultural, municipal, industrial and environmental uses" (Doherty et al., 2012).

Traditional form of transfer of water from agriculture is permanent (called buy-and-dry) which results in permanent dry-up of agricultural lands. There is an increasing concern that these water transfers may have negative third-party effects such as impacts to the agricultural supply, service, and processing sectors that are fundamental to agriculture-based rural economies. One strategy to mitigate these negative third-party effects is to employ alternative transfer methods (ATMs). Doherty et al., 2012 define ATM as "a structured agreement that allows for the transfer of water to a new use while minimizing the impact on the local economy, providing other funding sources to the agricultural user, and/or optimizing both the agricultural and

nonagricultural benefits of the remaining lands." The main aim of these methods is to avoid permanent dry-up of agricultural land, and to minimize the economic and environmental impacts due to loss of irrigated agriculture. ATMs include interruptible supply agreements, rotational fallowing, deficit irrigation, and water banking. ATMs that are intermittent in nature like rotational fallowing and water banking can be applied to mitigate drought effects, provide supplies to municipalities and for environmental uses, provide emergency supplies, and long-term conjunctive use (CDM, 2011). Water banking, authorized by the Colorado legislature in 2003, is one such ATM that is gaining popularity in the Western Slope.

1.1 Water Banking

A water bank is a compensated voluntary water sharing arrangement under the auspices of which participating agricultural water users can share water by temporarily foregoing their irrigation and transferring their water to other water users. It is a market-based approach in which the deposits and withdrawals to the water "bank" are subject to operational considerations of pricing, transaction and sharing arrangement duration defined appropriately for its successful operation. A water bank could operate as part of the demand management component to prevent downstream lakes like Lake Powell from going below minimum power levels. In the longer term, it could operate to prevent shortages under the Colorado River Compact or could also help in responding to a Colorado River Compact curtailment and its effects on critical post-compact users, that is, lands that are irrigated by pre-compact water rights could be temporarily fallowed, and the water could be transferred under a water bank to critical post-compact water uses (like municipalities, industries etc.).

Originally suggested by a group of ranchers from Colorado's Western Slope, water banking system to legally reallocate water could be practiced on a rotational basis to minimize agricultural economic and environmental impacts. Water bank participants could temporarily lease water from full-season or partial/split-season irrigation regimes to free up their water. According to a study conducted to predict water market participation by Cook and Rabotyagov (2014), irrigators were required to participate in a series of stated preference exercises with real monetary payoffs and it was found that with all other factors being equal, irrigators are more likely to accept partial/split-season than full-season leases.

Forage and pasture crops are ideal for inclusion in a water bank because they are low-value crops, more tolerant to water stress, and usually do not experience much long-term effects on future production (MWH, 2012). Grass and alfalfa pasture crops are also primary irrigation water users on the Western Slope (MWH, 2012).

Beneficial *consumptive use* (CU) is the basis, measure and limit of a water right (Hobbs, 2003). It is defined as the amount of water withdrawn from a source (e.g., diversions) that is no longer available because it has been beneficially removed from the immediate water environment. Beneficial is used in the context such that water use is for benefit of humans and community, without any waste. The water returned to the water source through run-off and/or percolation, collectively termed *return flow*, is not considered to be consumptive use. Water conserved on a particular agricultural parcel for successful transfer under a water bank can only come from consumptive water used historically under a water right at that particular agricultural parcel. According to CWCB (2007), it is the reduced CU as compared to historical CU, and not the

reduction in gross diversions that can be potentially transferred to other water users. *Conserved CU* is therefore defined as the amount of water that is a part of the consumptive use of a water right that is removed from an irrigated agricultural parcel. Conserved CU, based on reduced CU due to temporary decrease relative to historical consumptive use, would be available to a water bank for meeting Colorado River Compact obligations and/or transfer to downstream junior water users.

Conserved CU = Historical CU – Reduced CU (1.1)

1.2 Measuring and Monitoring CU

The precise amount of water consumed is important to be quantified for proper water management under a water bank, especially as the demands of water increase and puts pressure on limited water resources. It is essential to accurately measure and monitor changes in CU to develop reliable water sharing agreements. This is an important distinction for intermittent reliability sharing agreements like water banks because net benefits are smaller than that of permanent water transfers (Colby et al., 2014). Innovative and improved measuring of temporary water transfers could reduce costs of monitoring water transfer and increase reliability (Colby et al., 2012).

Effective water transfers in the past have been limited by their credibility in monitoring and measuring changes in CU (Keplinger and McCarl, 1998; Young 2010; Colby et al., 2014). Klamath Water Bank in Oregon was limited by the lack of proper monitoring and measuring technology, and the precise impact of water banking systems was not captured because even though the streamflow increased by temporary fallowing, the increase was within streamflow measurement error and couldn't be quantified (USGS, 2005; GAO, 2005). Other water transfer

proposals in the past were prohibited for groundwater-irrigated fields, fields near canals causing water seepage, fields with deep-rooted crops like alfalfa or with shallow groundwater (Colby et al., 2012). This is because, even if reliable records are available, CU (both historic and reduced) may not necessarily be equal to values obtained from these records.

Water consumed by crops in the form of CU is essentially utilized in transpiration from the stomata from the leaves, and in crop growth and metabolism. The amount of water required in growth and metabolic processes is quite insignificant as compared to transpiration. The water stored on the surface of agricultural fields is also lost in the form of evaporation. Evaporation is extremely difficult to measure separately from transpiration. Also, evaporation cannot be influenced independently of transpiration within a crop micro-environment. Therefore, the two processes are considered together and called evapotranspiration (Taylor and Ashcroft, 1972). Thus, crop CU is practically equivalent to evapotranspiration (ET) (Michael, 1978). The following sections discuss methods to determine CU or ET.

1.2.1 Traditional Methods

This section describes the common traditional methods used for quantifying agricultural CU, namely, water delivery-based method, reference/potential Penman-Monteith method, and estimation from point-based soil moisture sensors.

Water delivery-based method is based upon the water delivery data collected by gauges installed at the headgates of agricultural parcels. Not all agricultural parcels have these measuring gauges, especially in the past, thus limiting the historical water delivery records. Besides, these records may not be accurate enough, as mentioned in McIntire (1970) and USGS (2005). The diversion

measurement system has undergone improvement in terms of automated control and improved delivery management in the last couple of years. But, seepage, tailwater and return flows from agricultural parcels may not be accounted for in these water delivery-based methods, as was discussed in the last section.

Penman-Monteith method is recommended to be adopted as a standard for estimating reference ET because it closely estimates potential water use for reference crops and is physically-based (Allen et al., 1998). Methods previously used like Blaney-Criddle are found to have variable adherence to ET of reference crops (Allen et al., 1998). Penman-Monteith method estimates ET under potential/ideal vegetation conditions with extensive surfaces of no water shortage. The reference ET can be determined for either of the standardized reference crops - that is for grass (short crop) or alfalfa (tall crop). Grass reference ET (ET_o) is defined as the ET of an actively growing, densely vegetated cool season grass of 0.12 m height that is spread over an extensive surface and is not short of water. Alfalfa reference ET (ET_r) is defined as the ET of an actively growing, densely vegetated full cover crop of 0.50 m height that is spread over an extensive surface and is not short of water. Extensive surface refers to expanse of same vegetation for at least 100 m. The reference ET incorporates the effect of weather by considering standard vegetation surfaces. The standardized Penman-Monteith equation as described in ASCE – EWRI (2005) is given below:

$$ET_s = \frac{0.408\,\Delta\,(R_n - G) + \gamma \frac{C_n}{T + 273} u_2 (e_s - e_a)}{\Delta + (1 + C_d\,u_2)} \qquad (1.2)$$

where ET_s is the reference ET for standard crop (ET_o for grass and ET_r for alfalfa) and the units are in mm/hour for hourly time step and mm/day for daily time step. On the right hand side of the equation, R_n is the net radiation at the crop surface (MJ/m^2/hour for hourly time step and

$MJ/m^2/day$ for daily time step), G is the soil heat flux at the ground ($MJ/m^2/hour$ for hourly time step and $MJ/m^2/day$ for daily time step), u_2 is the average hourly or daily wind speed at a height of 2 m (m/s), e_s and e_a are the saturation and actual vapor pressures (kPa), respectively, T is the average air temperature (˚C), Δ is the slope of saturation vapor pressure-temperature curve (kPa/˚C), and γ is psychrometric constant (kPa/˚C). C_n (K mm s^3/Mg/hour or K mm s^3/Mg/day) and C_d (s/m) are constants that change with the time step (hourly or daily), and are specific for the type of reference crop (grass or alfalfa). C_n and C_d were derived by simplifying several terms within the Penman Monteith equation and rounding the result (ASCE - EWRI 2005). The constant C_n incorporates the effect of aerodynamic roughness of the reference surface. The constant C_d incorporates the effect of bulk surface resistance and aerodynamic roughness of the reference surface.

While the reference ET is determined by climatic conditions, differences in crop canopy, crop height, albedo, and stomatal and aerodynamic characteristics cause the transpiration of different crops to be different from reference crops. These differences are incorporated into a crop coefficient, which is different for different crops.

$$ET_c = ET_s \,.\, K_c \qquad (1.3)$$

where K_c is the crop coefficient and ET_c is the crop evapotranspiration under excellent disease-free, weed-free, insect-free, non-saline, well-fertilized fields of non-limiting soil water conditions. ET_c thus represents the upper envelope of crop evapotranspiration. The crop coefficient can either be a single crop coefficient (K_c) that averages the effect of evaporation and transpiration, or a dual crop coefficient (K_{cb} + K_e) that separately takes in to account basal transpiration and soil evaporation. The choice between the two depends on the purpose of

calculation, data available and the time step of computations (Allen et al., 1998). The single crop coefficient is used to calculate ETc for weekly or longer time periods like monthly, although dual crop coefficient for daily time steps summed up to weekly or longer time period can also be used. Single crop coefficient is recommended for planning and design of irrigation systems, while duel crop coefficient is recommended for irrigation scheduling (Allen et al., 1998). The crop coefficients are not only dependent upon crop properties, they also vary with climatic conditions. Because of this reason, the mid-season tabulated FAO-56 crop coefficients ($K_{cmid(tab)}$) originally developed at sub-humid climatic conditions need to be adjusted using the equation below, as described in Allen et al., 1998:

$$K_{c_{mid}} = K_{c_{mid(tab)}} + [0.04(u_2 - 2) - 0.004\,(RH_{min} - 45)]\left(\frac{h}{3}\right)^{0.3} \quad (1.4)$$

where K_{cmid} is the adjusted mid-season crop coefficient, h is the mean crop height in the mid-season growth stage, u_2 is the mean daily wind speed in the mid-season growth stage, and RH_{min} is the mean daily minimum relative humidity in percentage in the mid-season growth stage.

Estimation of ET from point-based soil moisture sensors is also a traditional way to estimate crop water use. Water inputs and outputs are traced in the soil using the following equation:

$$D_i = D_{i-1} + ET_a - P - I + DP - GW \quad (1.5)$$

where D_i and D_{i-1} are soil moisture deficits for present and previous day, ET_a is actual ET, I is net irrigation, P is effective precipitation, GW is upward groundwater contribution and DP is deep percolation. ETa is determined by inverting the above equation while all other variables are measured or assumed reasonably.

1.2.2 Remote Sensing

While traditional methods are limited in their capability to capture the spatial variability of actual ET over large areas, remote sensing can be particularly beneficial for determining crop water use (CU or equivalently, ET) over large spatial areas. Advances in earth observation systems have enabled remote sensing technology to be used beneficially to our advantage. Reflectance from the surface of the earth is measured by remote sensing platforms like satellites and aerial vehicles, and unique spectral signature of objects is used to delineate their properties. For example, healthy vegetation has a very high reflectance in Near Infrared (NIR) band and a low reflectance in Red band such that the difference between these two bands is high, while for bare soil, the difference between these two bands is relatively low (Gitelson and Merzlyak, 1996; Rock et al., 1986). Distinction between healthy and stressed vegetation is distinctively delineated in Red, NIR and Thermal Infrared (TIR) bands. Due to these unique spectral properties and distinctions, remote sensing can be utilized to monitor crop health and water status.

Numerous remote sensing-based ET algorithms that vary in complexity for estimating magnitude and trends in crop water use exist. Remote sensing from remote platforms like satellites has long been recognized as the most feasible method to monitor spatially-distributed crop water use over large areas (Gowda et al., 2008; Jackson et al. 1984). Quantifying the consumption of water over large areas such as irrigated agricultural areas is important for water resources planning, establishment of hydrologic water balances, water transfer and regulation (Allen et al. 2011). Remote sensing techniques have been proven reliable for assessing crop water use at different spatio-temporal scales (Gowda et al., 2008). According to Gowda et al. (2008), remote sensing techniques to estimate ET fall under two categories, land surface energy balance and reflectance-based crop coefficient approach, as is discussed below.

1.2.2.1 Land Surface Energy Balance

This approach is based on the law of conservation of energy which states that the total amount of energy in a system is conserved, although energy within the system can be changed from one form to another or transferred from one object to another. On land, the net energy (that is the net radiation (Rn)) is converted to other forms of energy like sensible heat (H), ground heat (G), and latent heat (LE) fluxes. Evapotranspiration consumes energy from the environment and this energy is the LE. The basic energy balance is given below:

$$R_n = H + G + LE \quad (1.6)$$

This basic energy balance equation is inverted to determine LE and thus ET as a residual after determining the rest of the components, that is,

$$LE = R_n - H - G \quad (1.7)$$

The concept of energy balance to determine heat balance of earth's surface (Budyko et al., 1961), evaporation (Fritschen and Bavel, 1962), and evapotranspiration under non-water limiting conditions (McNaughton and Black, 1973) has been around for many decades, but it is the recent advances in estimating sensible heat flux (H) that has enhanced the accuracy significantly (Taghvaeian et al., 2011). Sensible heat flux takes place due to the temperature gradient between plant canopy and the surrounding air. It is one of the most critical parts of solving the energy balance, and is mathematically defined as:

$$H = \rho C_p (T_{aero} - T_a) / r_{ah} \quad (1.8)$$

where, ρ is the density of air, C_p is the specific heat of air, r_{ah} is the surface aerodynamic resistance to heat transfer, T_{aero} is the surface aerodynamic temperature, and T_a is the air temperature at screen height (Brutsaert et al., 1993). Even though the equation to determine H looks simple, T_{aero} cannot be measured. Remote sensing TIR band detects radiometric surface temperature (T_s), which is different from the surface aerodynamic temperature (T_{aero}). The two

temperatures have been found to differ by 1-5 ˚C, mostly as a function of canopy density, height, wind speed and solar angle (Qualls and Brutsaert, 1996; Qualls and Hopson, 1998). Merely a difference of 1 ˚C can result in ET difference of 1mm/day (Campbell and Norman, 1998; Irmak et al., 2012).

The pioneering approach that enhanced the accuracy of estimating ET (Taghvaeian et al., 2012) is called "Surface Energy Balance Algorithm for Land (SEBAL)" by Bastiaansen et al., 1998. In this, the temperature differential ($T_{aero} - T_a$) in equation (1.8) is replaced with dT, which is then modelled as a linear function of radiometric surface temperature (T_s). To solve the linear function, inverse calibration at two extreme conditions of evaporative cooling is done. This inverse calibration assumes that over a wet agricultural surface (called the cold surface/pixel), all of the available energy ($R_n - G$) is used for ET and the temperature differential is negligible. Conversely, over a very dry agricultural surface (called hot surface/pixel) like bare agricultural soil with severe water limitation, the ET is negligible. Spatially anchoring these two extreme surfaces/pixels for inverse calibration enables interpolation of H of all surfaces in between, and eliminates the need to determine T_{aero} (Bastiaanssen et al., 1998). Since remote sensing provides a snapshot at a particular time (hour) in the day, the instantaneous (hourly) estimates need to be extrapolated to daily values. In SEBAL, this is done on the basis of assumption of constancy of instantaneous ET to instantaneous available energy ratio over the day, especially for cloud-free sky conditions (Brutsaert and Sugita, 1992). This ratio is called evaporative fraction (EF). However, according to Gentine et al. (2011), EF rarely remains constant throughout the day. According to Gowda et al. (2008), EF assumption might not hold in arid and semi-arid regions where advection is common.

An improved modification of the SEBAL model is “Mapping Evapotranspiration with Internalized Calibration (METRIC)” that is based upon the same principles as SEBAL, but the main difference lies in the calibration (Allen et al., 2007a, Trezza et al., 2002). Instead of assuming all available energy consumed for ET at the cold pixel, it assumes cold pixel ET equal to 1.05 times of alfalfa reference hourly ET calculated from nearest weather station; and for the hot pixel, instead of assuming ET to be negligible, it suggests doing a daily surface soil water balance to confirm if ET equals zero or to supply a non-zero value for ET if there is residual evaporation from antecedent precipitation or wetting event. For extrapolating from instantaneous (hourly) to daily, instead of EF, METRIC uses ET reference (alfalfa) fraction (ETrF) which is the ratio of remotely sensed instantaneous ET to reference ET at that instant. This ratio is essentially equal to actual crop coefficient, which does not vary from instantaneous to daily time scale, and thus can be used for estimating daily ET from remote sensing (Trezza et al., 2002).

A further modification of SEBAL and METRIC is the “Remote Sensing of Evapotranspiration (ReSET)” model that explicitly takes into account the spatial variability in the weather data (Elhaddad and Garcia, 2008 and 2011). Tasumi (2003) mentioned that variable wind speeds in an image to be processed are a challenge because surface temperature and dT may change with wind speed. Wind speed affects the estimation of the surface aerodynamic resistance for heat transport (r_{ah}) that impacts the dT function, and thus the accurate estimation of H. Selecting a local hot pixel for each region is essential because of this reason. Therefore, instead of a hot pixel representing a constant upper temperature condition at only one point, this raster approach uses a hot grid that is an interpolation from several hot pixels representing the spatial variation in conditions over the target area. The same concept applies to cold pixels. (Elhaddad and Garcia

2011). ReSET can be run in either calibrated mode, or in uncalibrated mode, depending upon the weather data available. The calibrated mode is similar to METRIC in which the reference ET from weather stations is used to set the maximum ET of the cold pixel in the image, and the uncalibrated mode is similar to SEBAL where no maximum ET value is imposed (Elhaddad et al., 2011). In both of these modes, the internal calculations are rasterized such that each pixel is modeled on the basis of its spatial location.

ET estimation for periods longer than daily requires interpolation between consecutive overpass daily ET estimates. While originally SEBAL did a linear interpolation, METRIC prefers interpolation for ETrF for non-overpass days, using curvilinear interpolation functions like cubic spline that better fit typical curvilinearity of crop coefficients in a growing season (Allen et al., 2011). ReSET interpolation between two consecutive overpass dates includes a linear interpolation while taking into account spatio-temporal variability in weather data (Elhaddad and Garcia, 2008).

SEBAL has been utilized worldwide and its typical accuracy, on average is 85% for daily and 95% for seasonal ET estimations. Applications of SEBAL in Idaho by Trezza et al. (2002) revealed accuracies ranging from 65% to 97.3%, with an average accuracy of 81.8%. SEBAL may not be able to capture advection and thus may underestimate ET. In this case, a modified SEBAL model called SEBAL-A (Mkhwanazi et al., 2015a) can be used in areas of limiting weather data and advective conditions. For irrigated surfaces with advective conditions where SEBAL errors were significantly higher, SEBAL-A performed better with a daily accuracy higher than 85% (Mkhwanazi et al., 2015b). METRIC has been validated in Idaho for different

crop conditions- daily ET estimation errors were in the range of 10-20%, and error over a 4-month period reduced to 4% (Allen at al., 2005; Allen et al., 2007; Gowda et al., 2008). ReSET error estimated relative to a local lysimeter in Bushland, Texas was 13.6% for uncalibrated mode and 11.6% for calibrated mode, on a daily basis (Elhaddad et al., 2011).

Besides the one-source models discussed above, other energy balance models include two-source or two-layer models which consider canopy and soil fluxes separately, and multi-layer models that divide the canopy into many layers. Among these, the Two-Source Model (TSM) developed by Norman et al. (1995) and Kustas and Norman (1999) has been applied in several studies. This approach in addition to weather and remote sensing data (thermal and multispectral bands) requires some knowledge of crop and requires assumptions such as partitioning of composite radiometric surface temperature into soil and vegetation components, turbulent energy and mass exchange at soil level and coupling/decoupling of soil and canopy (parallel or series network) (Gowda et al., 2008). Gonzalez-Dugo et al. (2006) compared ET obtained from TSM with eddy covariance ET estimates and found the regression between them equal to 0.94. According to French et al. (2015), implementation of TSM involves many assumptions, is sensitive to land surface temperature observation errors, and is recommended when crop biophysical surface conditions are known.

1.2.2.2 Reflectance-based crop coefficient approach

More complex ET methods are not necessarily more accurate than empirical approaches (Kalma et al. 2008). Reflectance-based crop coefficient is an empirical approach in which actual crop coefficients based on field conditions are empirically modelled by vegetation indices. Vegetation indices (VIs) are mathematical combinations of different bands in the electromagnetic spectrum

(mostly in Visible and Infrared) and are used to distinguish vegetation biophysical properties. NDVI is a normalized difference vegetation index that uses NIR and Red bands of electromagnetic spectrum. It was developed by Deering (1978), and is given by the following equation:

$$\text{NDVI} = \frac{\text{NIR}-\text{Red}}{\text{NIR}+\text{Red}} \quad (1.9)$$

In reflectance-based cop coefficient approach, first step is to obtain spatially-distributed crop coefficient from reflectance data, that is, from VI calculated from reflectance in specific bands. For this, a locally developed empirical relation between VI and crop coefficient is needed- this relation is empirical because biomass, crop fractional cover and thus crop coefficients can be related and tracked by VIs. Since these crop coefficients are based upon actual reflectance data they are considered to determine actual crop conditions in a field. These reflectance-based crop coefficients (Kcr) can then be multiplied with reference ET from the nearest weather station to determine actual water use without the need of a thermal band.

Several previous studies have developed VI-Kc (or Kcb, when evaporation is known to be negligible) functions for different crops over different areas. These include relations developed for corn (Neale et al. 1989; Bausch 1993), wheat (Ray and Dadhwal 2001), cotton (Hunsaker et al. 2003), potato (Jayanthi et al. 2007), soybean, sorghum, and alfalfa (Singh and Irmak 2009). The table below (Table 1) gives these already developed relations for different crops and the studies in which each of them were developed. Er-Raki et al. (2007) evaluated this approach for winter wheat in Morocco and found the efficiency of this approach to be 70-80%, compared to 44% of that of FAO-56 procedure (Gowda et al., 2008). Neale et al. (2003) concluded that the

remote sensing based crop coefficients can be accurately used for grain, non-grain and forage crops.

Table 1 VI-Kc (or Kcb) relations from past studies

Study	Area	Crop	Relation
Neale et al. (1989)	Colorado,US (Fruita)	Corn	Kcb=1.092NDVI-0.053
Bausch et al. (1993)	Colorado,US (Fort Collins)	Corn	Kcb=1.416SAVI+0.017
Ray & Dadhwal (2001)	Gujarat, India	Early Wheat Late Wheat Perennials	Kc=1.904SAVI-0.401 Kc=2.004SAVI-0.159 Kc=0.895SAVI+0.280
Hunsaker et al. (2003)	Arizona, US	Cotton (pre full cover)	Kcb=1.49NDVI - 0.12
Jayanthi et al. (2007)	Idaho, US	Potato	Kcb=1.085SAVI+0.05
Singh & Irmak (2009)	Nebraska, US	Irrigated corn Irrigated soybean Irrigated sorghum Irrigated alfalfa	Kc=1.31NDVI+0.027 Kc=1.22NDVI+0.033 Kc=1.34NDVI-0.056 Kc=0.981NDV+0.113

1.3 Remote Sensing Platforms

Remote sensing platforms can be space-borne, air-borne or ground based. For large spatial coverage, space-borne and air-borne platforms are preferred. While air-borne platforms like manned or unmanned aerial vehicles to fly over desired areas for collecting remote sensing data are not very common yet, space-borne earth observation satellites (EOSs) have unrestricted ability to cover earth's surface repeatedly. Earth observation satellites range from low resolution

(AVHRR, MODIS, ASTER, etc.) to moderate resolution (Landsat, Sentinel, SPOT, etc.) to hyperspatial (high) resolution (commercial satellites like Ikonos, Worldview, GeoEye, Quickbird, etc.) and hyperspectral satellites (Hyperion etc.). Some common EOSs that are utilized for earth observation, with their bands, resolutions and revisit periods, are given below in Table 2.

Table 2 Common Earth Observation Satellites

Satellite	Time of operation	Bands (of EM spectrum) included	VIS, NIR band resolution	Thermal band resolution	Revisit time period
MODIS	December 1999 - present	36 bands, from 0.4 to 14.4 um	250 m for NIR and Red ; 500 m for Blue, Green and 3 IR bands	1 km	~1 day
AVHRR	NOAA-12 AVHRR from September 1991 - present	Red, NIR, SWIR, TIR	1.1 km	1.1 km	1 day
Landsat 5	March 1984 - November 2011	Blue, Green, Red, NIR, 2 SWIR, TIR	30 m	120 m	16 days

Landsat 7	April 1999 - present	Blue, Green, Red, NIR, 2 SWIR, Panchromatic, TIR	30 m	60 m	16 days
Landsat 8	March 2013 - present	Blue, Green, Red, NIR, SWIR, Panchromatic, TIR	30 m	100 m	16 days
Sentinel 2a Sentinel 2b	June 2015 (collecting data since November 2015) – present 2017(expected)	13 bands in Visible, NIR and SWIR same as Sentinel 2a	10-60 m (changes with bandwidth) -	- -	~10 days Combined with Sentinel 2a, approximately 5 days
Ikonos	September 1999 - present	Blue, Green, Red, NIR,	4 m	-	Appx. 3 days

		Panchromatic			
Quickbird 2	October 2001 - present	Blue, Green, Red, NIR, Panchromatic	2.44 m	-	1-3.5 days, depending on the latitude

Depending on the type of use and methodology, appropriate satellites can be selected. While data from satellites like MODIS, Landsat, Sentinel 2a etc. can be obtained at no cost, high resolution (hyperspatial) data from commercial satellites like Ikonos, Quickbird, Worldview etc. is not free of charge.

1.4 Problem Statement

The quantification of precise amount of water uptake by agricultural crops, or, consumptive use, is crucial for water management for the Colorado River Basin. Reliable and accurate CU (or ET) estimates over large areas for a sharing arrangement like a market-based water bank in the Western Slope of Colorado becomes even more crucial because of the temporary and intermittent nature of water sharing, where the net economic benefits of temporary transfers are small compared to the outright purchase of agricultural water rights. Any water conserved, or conserved CU (CCU) would serve as the fundamental basis of compensation to agricultural water users who participate in a market-based water bank. Because CCU is based on reduced CU relative to historical (or full) CU, accurate spatial estimates of water beneficially used is necessary for both historical (full, or no water limitation) and water-limited conditions. Traditional point-based measurements do not capture intra and inter- field variability, and water-delivery records - even if available for most of the parcels in the area- may not be reliable enough, and do not differentiate between consumptive and non-consumptive uses. Potential

methods like Penman-Monteith estimate reference ET under ideal agronomic conditions in the soil (which may not always exist), accuracy of which also depends upon accuracy of crop coefficients and length of growth stages specific to a given location and climate.

Previous research studies recognize Remote Sensing as the most feasible method to determine spatial crop water use over large areas (Gowda et al., 2008). According to Ambast et al. (2002), there is still a gap between research studies and practical application of remote sensing techniques for water management. Earth observation satellites, which have been operational since the late half of the twentieth century offer an opportunity to reliably assess actual ET, as determined from actual radiation reflected and emitted from the agricultural fields.

ReSET has been applied successfully on the Eastern Front Range of Colorado for crops like corn, alfalfa, etc. It has not been utilized or applied for pasture crops in geographically diffused agro-climatological areas of the Western Slope. Since it has a potential to be used for reliable CU, performance of this model as it applies to Western Slope needs to be evaluated for both energy-limiting (non soil-water limiting) and soil-water limiting conditions.

While energy balance approach requires the coarser thermal band and follows a physically-based approach, reflectance based crop coefficient approach is empirical but can afford higher spatial resolution without the need of the coarser thermal band. This may be required for capturing intra-field variability, and maybe especially applicable for smaller pasture fields in the Western Slope where coarse thermal resolution is a limitation and energy balance method cannot be applied without some contamination of the thermal pixel from surrounding areas. A VI-Kc model for

grass pastures has never been developed before. Potential of utilizing this approach needs to be assessed.

1.5 Objectives

The objectives of this study are as follows:

1. Performance evaluation of ReSET for agro-climatological conditions of Western Slope of Colorado
2. Determine monthly CCU from ReSET
3. Determine local crop growth stage lengths for different cutting cycles for grass and alfalfa pastures
4. Develop VI-Kc model for grass pastures for use with reflectance based crop coefficient method
5. Evaluate reflectance-based models for grass and alfalfa pastures on a daily basis

CHAPTER 2: MATERIALS AND METHODS

2.1 Study Area

The overall study area comprises the Uncompahgre and Gunnison area of the Western Slope of Colorado (shown in figure 1). The elevation of the region varies from about 1400 m to about 3000 m. Precipitation and temperature varies with elevation resulting in differences in crop evapotranspiration, effective precipitation, and consumptive water requirements. Major rivers that flow in the area are the Uncompahgre River which drains into the Gunnison River, which eventually drains into the Colorado River. While the Uncompahgre region is at a lower elevation (on an average of about 1700 m), Gunnison is at a higher elevation (on an average of about 2400 m). The agro-climatological conditions of both areas differ widely due to different elevations and diverse hydrological conditions. The most common irrigation methods in the study area are surface irrigation, with flood irrigation (where water is released onto a field, and allowed to flow along the ground through gravity) more prevalent for Gunnison agricultural fields. The crops of focus for this study are grass and alfalfa pastures because they together occupy a major part of irrigated agriculture in the study area and are economically fit for a water bank (MWH, 2012).

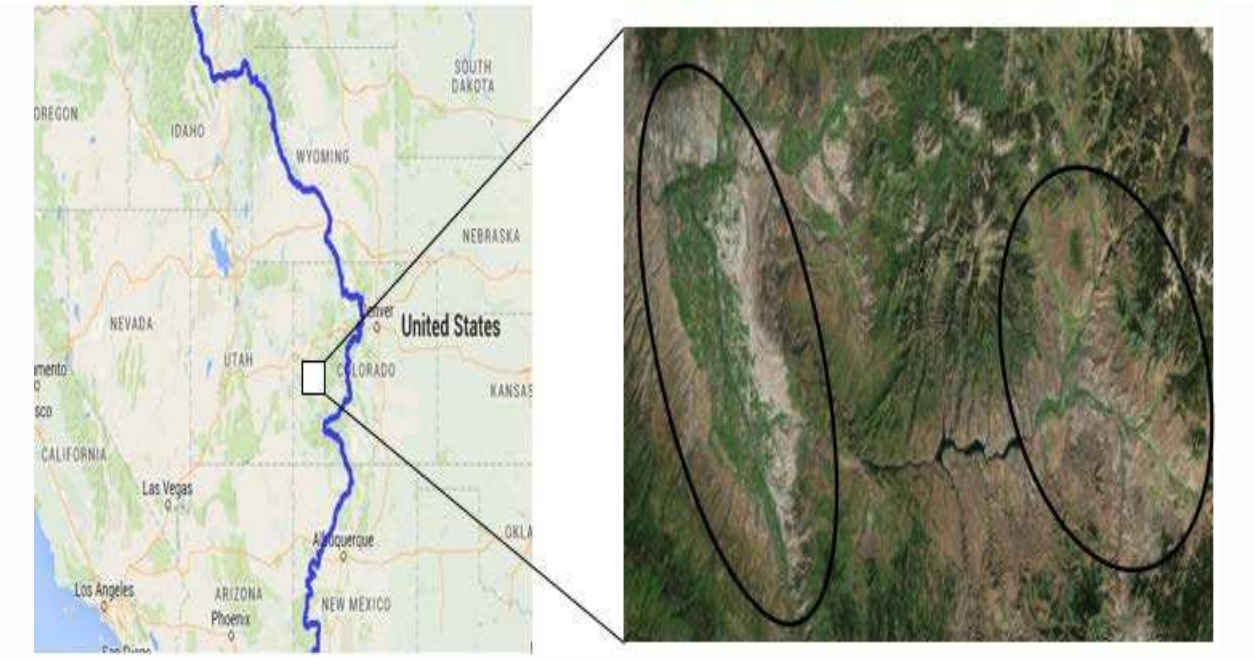

Figure 1 Study area; Zoomed in- Uncompahgre on left and Gunnison on right

A grass pasture site at Montrose (in Uncompahgre region) was selected to evaluate ground estimations of remotely sensed CU. This site is located approximately at 38.509˚ N and -107.874˚ W and at an elevation of about 1,760 m above mean sea level. The size of the field is 14.5 acre (58,680 m^2), and consists of fescue, orchard grass, alfalfa smooth broome, wheatgrass, bluegrass and plantago grass types. It is divided into two treatments - full irrigation (replicating full irrigation conditions of the past, under the terms of a water right), and limited/split-season (replicating potential water bank scenario where irrigation is applied only for partial season). This is shown in figure 2, the treatment plot on the left was fully irrigated (reference) and the treatment plot on the right was limited-irrigated. The soil type at full treatment plot is clayey loam and at partial treatment plot is clayey. The full irrigation plot was irrigated throughout the growing seasons of 2015 and 2016, while irrigation at partial treatment plot irrigation was stopped at start of August in 2015 and July in 2016 growing season. On the limited irrigation

treatment plot, a Kipp and Zonen Large Aperture Scintillometer (LAS), along with a Kipp and Zonen NR Lite 2 Net Radiometer, and HFT 3.1, Radiation and Energy Balance Systems, Inc Soil heat flux plates were installed to measure sensible heat flux, net radiation and ground heat flux, respectively, so that as a result of these measurements, ET flux can be calculated. These sensors were installed from August-October in 2015 and June-October in 2016.

Figure 2 Montrose site; Reference treatment plot on left and Limited treatment plot on right

2.2 Satellite Data

Landsat 8 and 7 satellites' imagery (downloaded from www.earthexplorer.usgs.gov) was used to run the energy balance because they have the finest thermal resolution among all the other satellites with a thermal band. Two Path/Row combinations encompassing the study area were processed. The overpass for the Uncompahgre region is Path 35/Row 33, and over the Gunnison region is Path 34/Row 33 – both of which are respectively shown in figures 3 and 4. Each of these images covers an area of 160 km x 160 km. Since these are both consecutive overpasses,

there is an overlap between the two. A large part of the western Gunnison area falls on this overlap. The time difference between the two overpasses is 1 day. While Landsat 7 images have stripes because of the Scan Line Corrector failure in 2003, half of the Uncompahgre region (including the Montrose study site) lies at the center of the scene and is free of striping issues. The cloud-free images processed for Uncompahgre overpass (Path35/Row33) were June 2, June 18, June 26, July 12, July 20, July 28, August 5, August 13, August 21, August 29, September 6, October 8 in 2015 ; and April 1, May 3, May 19, May 27, June 4, June 20, June 28, July 6, July 14, August 7 in 2016. The cloud-free images processed for the Gunnison overpass (Path 34/Row 33) were June 19, June 27, July 13, July 29, August 6, August 14, August 30, September 23 in 2015; and May 4, May 12, June 5, June 13, June 21, July 7, July 23 in 2016.

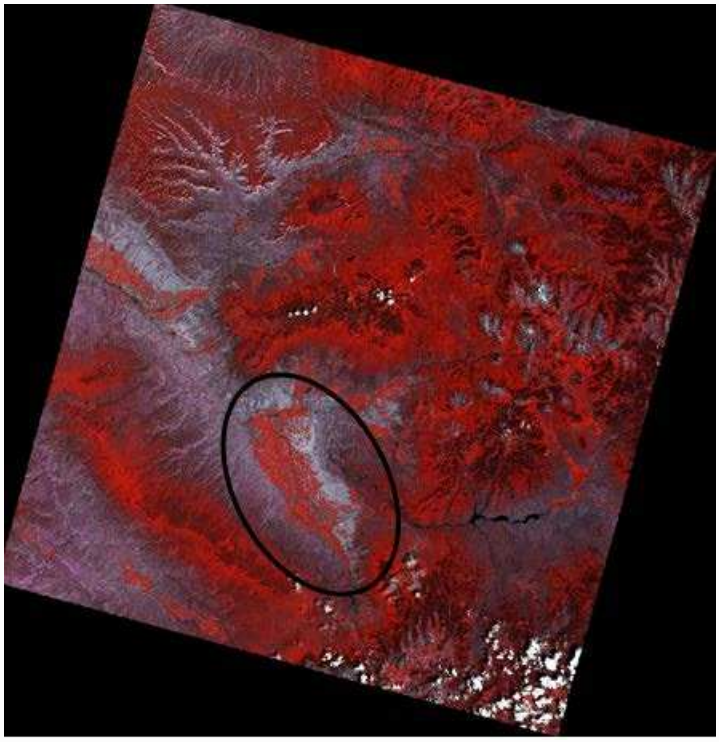

Figure 3 Landsat 8 imagery for Path35/Row33

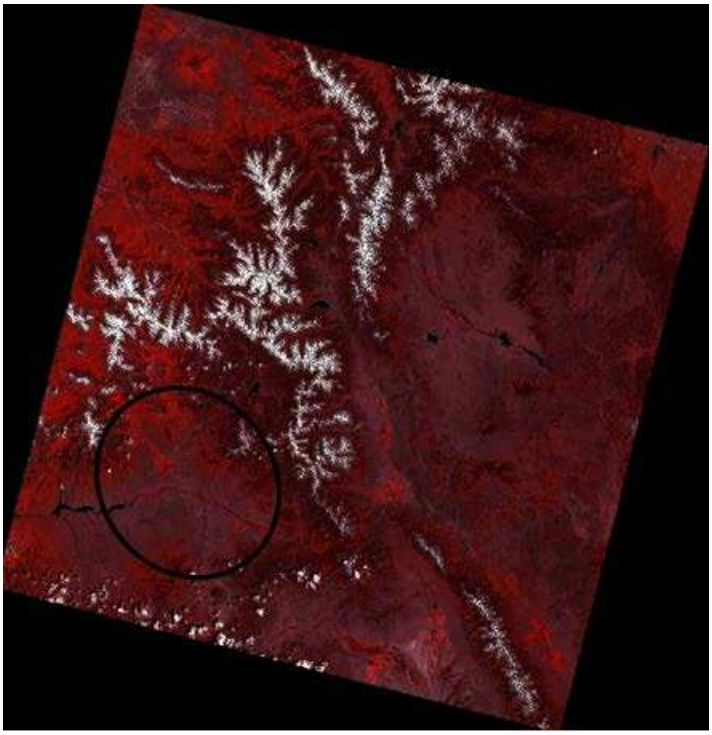

Figure 4 Landsat 8 imagery for Path34/Row33

Additionally, Sentinel 2a MSI data (downloaded from www.earthexplorer.usgs.gov), over the Uncompahgre, were utilized in the growing season of 2016. Sentinel 2a MSI overpass image used is shown in figure 5. The cloud-free images used were March 8, April 7, June 6, June 19, June 26, July 9, July 16, and July 29.

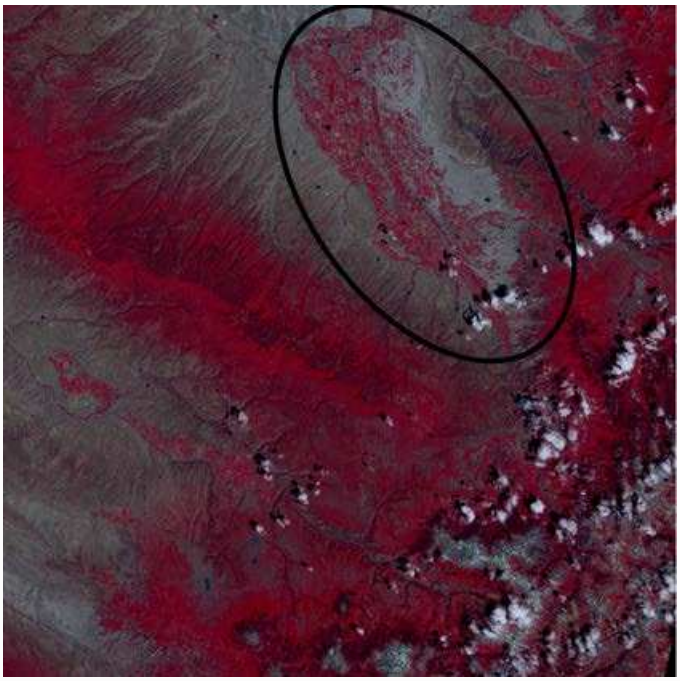

Figure 5 Sentinel 2a MSI -Uncompahgre overpass imagery

2.3 Weather data

Weather data were downloaded from Colorado Agricultural Meteorological (COAGMET) network of weather stations (http://www.coagmet.colostate.edu/). These weather stations measure weather variables like air temperature, relative humidity vapor pressure, solar radiation, wind speed and precipitation. Throughout 2015 and 2016 growing season, there were 9 functional weather stations (Appendix 1) encompassing the two overpass images. While most of these weather stations are in the Uncompahgre, there is only one weather station in Gunnison (installed in 2015). It is noted on the COAGMENT website that the threshold wind speed (minimum reading) for the weather stations' anemometers is 0.49 m/s (1.12 miles/hour or 26.84 miles/day). Values below this threshold are dropped to 0. The wind speed in the study area is generally low, often lower than 1 m/s, and sometimes even below 0.5 m/s (which is dropped by the anemometer).

2.4 Digital Elevation Data

Elevation of the Western Slope varies widely, which means that the short-wave radiation reaching the surface of earth varies widely and an atmospheric lapse rate correction is needed to take into account the net cooling of temperature aloft with elevation. Thus, a digital elevation model over the area is needed. National Elevation Dataset (NED) of 1/3 arc-second, which is approximately equal to 10 meters in the study area, was used.

2.5 Crop Cover Data

Crop cover classification map for 2015 was downloaded from USDA NASS Cropscape (http://nassgeodata.gmu.edu/CropScape/). Also, additional field-specific crop type data was collected from field visits in the Uncompahgre. This field data served as ground validation for grass and alfalfa crops. From the field data, it was found that in the Cropscape map, some alfalfa fields were incorrectly classified as corn and some grass pastures as either alfalfa or other hay/pastures, but corn fields were mostly accurate. Field-specific crop type data was not collected in Gunnison since majority of the crops are grass pastures, and Cropscape also identifies most of the fields as grass pastures.

2.6 Procedure

The procedure employed to meet the objectives of the study are discussed in the following sections. Each section covers procedure for one or more of the objectives specified above, not necessarily in the same order.

2.6.1 ReSET model

ReSET calibrated mode involving inputs of spatially-distributed reference ET (instantaneous as well as daily) and wind speed maps was utilized for both Uncompahgre (Path 35/Row 33) imagery and Gunnison (Path 34/Row 33) imagery. Even though the Uncompahgre area comprised of 8 weather stations and the Gunnison area had only one, data from all weather stations was used for both of the overpasses to create spatially distributed maps. These maps were created by determining both hourly and daily (24-hour) alfalfa reference ET from Penman-Monteith method at each weather station, utilizing wind speed data from each weather station, and spatially interpolating these using Inverse Distance Weighted (IDW) function. Daily reference ET at each weather station was calculated by summing up the hourly reference ET (calculated for each hour from equation 1.2) for the whole day rather than using daily time-step in equation 1.2, because substantial changes in wind speed, humidity, cloudiness etc. during the day can affect average daily estimates of the parameters of equation 1.2.

The ReSET model used was largely automated, including selection of calibration/anchor (hot and cold) pixels. The automatic selection of hot and cold pixels was done by creating NDVI and albedo masks, selecting top candidates of pixels from image histogram, conditioning top candidate pixels to be in a cluster of 8 similar surrounding pixels and by constraining cold pixel selection to be within 10-20 km radius around the weather station. The automatic selection of hot and cold pixels was checked visually for every image. This automated selection of anchor pixels worked well enough for most of the Montrose imagery, but not for Gunnison imagery because of the complex topography (mountainous), soil-mineral depositions, lots of narrow water bodies and shallow groundwater cooling down the ground surface. Because of this, it was determined to best select anchor pixels manually for Gunnison imagery.

The Digital Elevation Model was used for atmospheric lapse rate correction using the standard lapse rate of 0.0065˚C/m from International Civil Aviation Organization (ICAO). Since locations with higher elevations are at a lower temperature than lower elevation areas, the model may detect higher locations as having higher ET values. To correct this error, temperature was adjusted to compensate for the change in elevation, as given by the equation below:

$$T_{corr\_s} = (\mathrm{DEM} - \mathrm{datum}) * 0.0065 + \mathrm{Ts} \quad (2.1)$$

Where, T_{corr_s} is the corrected surface temperature in Kelvins, T_s is the original radiometric surface temperature in Kelvins, DEM is the digital elevation data (in m) at any pixel and "datum" is the average elevation of the area of interest (1700 m for Uncompahgre, and 2400 m for Gunnison), as mentioned in Allen et al. (2011). Implication of datum selection and sensitivity of model to the datum value chosen over different spatial locations was not considered in this study, but needs to be assessed in future research.

For wind speed lower than 1m/s (either due to actual low wind or values dropped by the anemometer), the surface aerodynamic resistance (rah) term in the sensible heat flux equation (equation 1.8) breaks apart because of numerical instability because it is based on turbulence (good mixing) created by the interaction of wind with surface elements. Therefore, for missing wind speed below 1m/s (no data or otherwise), an assumption of wind speed equivalent to 1 m/s was made before spatially interpolating wind speed and utilizing wind speed map in the model. Because an assumption of wind speed is necessary, a wind sensitivity analysis was done to check if increasing the wind speed has a significant difference on daily ET estimations. The sensitivity analysis was carried out for 3 different wind speeds – 1, 1.4 and 1.8 m/s. This was done only for 2015 Path 35/Row 33 imagery, and the resulting analysis was done for the two treatment plots at

the field site at Montrose. Also, it is noteworthy to mention that since wind speed in the area is quite low, advection effects on energy balance would be minimum.

After determining instantaneous (hourly) ET at the time of overpass, the alfalfa reference evapotranspiration fraction (ETrF) mechanism was used to extrapolate instantaneous (hourly) ET to daily, as in Allen et al. (2007a). ETrF is the ratio of remotely sensed instantaneous ET (ET_i) to the grass reference ET (ET_{ref}) computed from weather station data at the time of satellite overpass.

$$\mathrm{ETrF} = \frac{\mathrm{ET_i}}{\mathrm{ET_{ref}}} \quad (2.2)$$

This ratio is essentially the actual grass-based crop coefficient, which does not vary from instantaneous to daily time scale, and was used to estimate daily ET_d by using the following equation:

$$\mathrm{ET_d} = \mathrm{ETrF} \,.\, \mathrm{ET_{d\_ref}} \quad (2.3)$$

where ET_{d_ref} is the daily grass reference ET calculated from weather station. These calculations are done in raster form, on a pixel-by-pixel basis. For interpolation between two consecutive overpass days to get monthly ET (for monthly CU estimates), correction ratio (γ) method, as mentioned in Elhaddad and Garcia (2008) and given below, was implemented.

$$\gamma = [(\mathrm{ETrF_i} - \mathrm{ETrF_{i+1}})/\mathrm{N}] \quad (2.4)$$

$$\mathrm{ET_{d\_i}} = [\,\mathrm{ETrF_i} - (\gamma * \mathrm{T})] * \mathrm{ET_{d\_ref}} \quad (2.5)$$

where $ETrF_i$ and $ETrF_{i+1}$ are the ETrF grids of two consecutive overpass days between which interpolation is being done, N is the number of days between the overpass images for which the data is being interpolated, ET_{d_i} is the interpolated daily ET between two consecutive overpass dates and ET_{d_ref} is the daily reference ET for that particular date. The ET_{d_i} changes for each

day, depending on where that day falls between the beginning and end of the interpolation period (T). This interpolation was done only for Montrose field site treatments to estimate monthly CCU when the limited treatment plot was stressed in 2015 and 2016.

Preliminary evaluation of ReSET ET daily assessments was done using two separate criteria; the first was utilizing ground instruments (LAS setup). LAS suite of instruments were installed only at the limited treatment plot to evaluate stress-condition ET because stressed vegetation has lower vegetation cover that leads to heterogeneity of surface, which creates a discrepancy between actual and ET estimated from models like ReSET that are based on big-leaf approach. Unfortunately, LAS measurements were not always made (or made accurately) because issues of alignment, low battery, etc., disrupted continuous good quality data collection. Nonetheless, 7 dates that overlapped with satellite overpass were identified, and daily ET was compared with ReSET derived-ET estimates at limited plot.

The second evaluation criteria was a scene-based evaluation in which the ET of fully- irrigated alfalfa field(s) in the scene at the peak growth time period was compared with ASCE reference ET. Since the reference ET is ideally the maximum weather demand, the maximum value of crop coefficient at these fully-irrigated alfalfa field(s) at peak growth should be reasonably close to 1. Fields with normal growing conditions (without any water or agronomic limitations) were chosen on the basis of a three-step filtering procedure. First, an inward buffer inside each field was implemented to minimize pixel contamination from surrounding roads, buildings or water bodies. Second, the NDVI filtering was done such that selected fields had NDVI higher than 0.75. Third, the highest crop coefficient pixel had to pass the clustering filter (3x3 pixel) to

eliminate noise. This scene evaluation at peak growth was done for both Uncompahgre and Gunnison imagery on day(s) when crop was at/near peak growth. Since the Cropscape crop cover classification did not show a substantial number of alfalfa fields in the Gunnison, the same evaluation of maximum crop coefficient was performed on grass pastures instead.

2.6.2 Crop growth stage lengths

In previous studies like that of Taghvaeian et al (2011), actual crop growth lengths varied from the ones mentioned in FAO-56. Lengths of crop development stages in FAO-56 tables are indicative of general conditions, but may vary substantially from region to region, with climate, elevation, crop variety and planting date (FAO-56). Additionally, individual agronomic practices may also affect the crop growth stages. Since crop growth lengths of grass and alfalfa pastures in the Western Slope have not been determined and/or verified before, it was done using Landsat 8, Landsat7, and Sentinel 2a MSI satellites for the year 2016. This was achieved by tracking biomass changes using NDVI from multispectral bands of these 3 satellites combined. Utilizing the 3 satellites increased the temporal resolution to better capture NDVI changes. To avoid any classification error in crop cover layer, only ground-truthed grass fields were assessed. Another filtering procedure was used in the process: An inward buffer of 60 m was created to avoid any edge effect. Fields that had a high intra-field standard deviation (>0.06 NDVI) and/or fields that didn't show much variation in NDVI throughout the season were eliminated because that meant non-uniform or poor growing conditions, or extensive grazing pastures. The crop growth lengths determined for each cutting cycle were analyzed, and compared to FAO-56 values.

2.6.3 Reflectance-based crop coefficient method and its evaluation

To use this simplified method that does not require thermal band, a VI-Kc relationship that is specific to a particular crop is needed. Since a VI-Kc relationship for grass pastures does not exist in the previous literature, it was developed using the data from the fields filtered in section 2.6.2. This was done by dividing the hourly ET raster derived from ReSET ($ET_{Reset_{hourly}}$) by the spatially-interpolated hourly alfalfa reference ET raster ($ET_{Ref_{hourly}}$) to obtain the Kc as shown in equation 2.6. Then, this Kc was regressed with NDVI for the corresponding fields for the same-day satellite overpass, to obtain an empirical reflectance-based model for grass pastures.

$$Kc_{Reset} = \frac{ET_{Reset_{hourly}}}{ET_{Ref_{hourly}}} \quad (2.6)$$

Furthermore, Reflectance based models for grass (developed in this study) and for alfalfa (developed in Nebraska by Irmak and Singh (2009); shown in Table 1) were compared with ReSET-derived daily ET estimates to evaluate their average daily performance on full and limited irrigation treatment plots (at Montrose) for grass, and filtered (in section 2.6.2) alfalfa field sites.

2.7 Statistical Evaluation

Coefficient of Variation (CV)

The Coefficient of Variation (CV) measures the variability in the values relative to the magnitude of the mean. It is a ratio of standard deviation and mean, often expressed in %.

Mean Biased Error (MBE) & Root Mean Square Error (RMSE)

$$RMSE = \left[N^{-1} \sum_{i=1}^{N} (P_i - O_i)^2\right]^{0.5} \quad (2.6)$$

$$MBE = N^{-1} \sum_{i=1}^{N} (P_i - O_i) \quad (2.7)$$

where, N is the number of observations, P is a prediction, and O is an observation. RMSE summarizes model error in terms of variance of magnitude and MBE describes model bias. The errors together can provide descriptive measures of model performance.

Nash-Sutcliffe Coefficient of Efficiency (NSCE)

It is used to assess the predictive power of a model's predictions with respect to observations, and is given by:

$$\mathrm{NSCE} = 1 - \frac{\sum_i^n (P_i - O_i)^2}{\sum_i^n (O_i - O_o)^2} \tag{2.8}$$

where, n is the number of observations, P is a prediction and O is an observation, and O_o is the mean of observations. The range of NSCE is from negative infinity to 1, with negative values indicating unacceptable model performance. The closer the value of NSCE is to 1, the more accurate a model is considered to be.

CHAPTER 3: RESULTS AND DISCUSSIONS

3.1 Performance and Evaluation of ReSET

3.1.1 Low (<1 m/s) wind speed

The probability distribution of wind speed at the time of satellite overpass for weather stations at/near Montrose for the growing season (April – October) of last 4 years is shown in figure 6. Similarly, the growing season wind probability distribution for Gunnison weather station since its installment in 2015 is shown in figure 7.

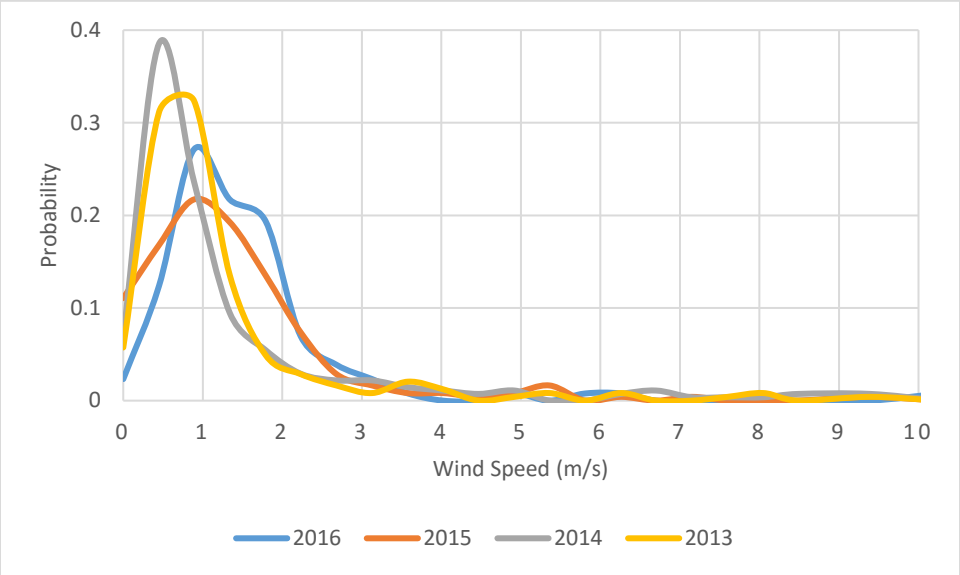

Figure 6 Montrose wind probability distribution from last 4 years

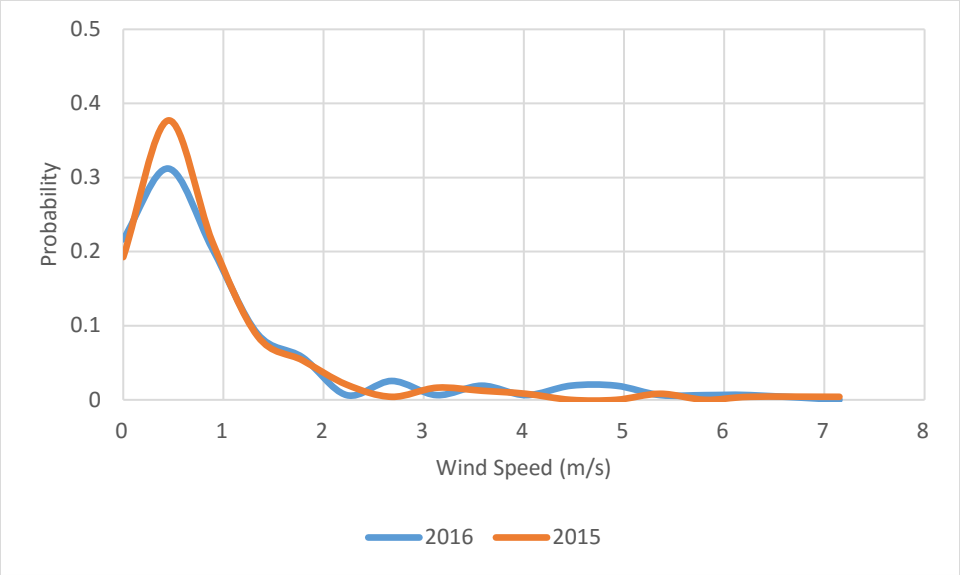

Figure 7 Gunnison wind probability distribution from last 2 years (since installment of weather station)

The distributions are positively skewed with about 60% and 75% of the growing season wind speed data, for Montrose and Gunnison respectively, being less than 1 m/s. While such low wind speeds are associated with minimum advection effects on energy balance, wind speeds lower than 1 m/s cause numerical instability in surface aerodynamic resistance (rah) term in equation (1.8). Therefore, for wind speed values lower than 1 m/s, at all weather stations in the study area, an assumption of 1 m/s was necessary. To test the effect of this assumption, the sensitivity of ReSET ET results to wind speed were analyzed, as discussed in section 3.1.2.

3.1.2 Wind Sensitivity Analysis

The sensitivity analysis was carried out for 3 different wind speeds: 1, 1.4 and 1.8 m/s. This was done only for 2015 Path 34/Row 33 imagery, and the result analysis was done for the two treatment plots at the field site at Montrose. Figures 8 and 9 show the percent coefficients of variation (% CV) of grass hourly ET for full irrigation and limited irrigation plot, respectively. The first bar (blue) in these figures represent the %CV between the hourly ETs obtained by

assuming a minimum wind speed of 1m/s and 1.4 m/s, for any wind speed values <1 m/s. Similarly, the second bar (yellow) is the %CV between the hourly ETs for 1.4m/s and 1.8 m/s. And, the third bar (red) is the %CV between the hourly ETs for 1m/s and 1.8 m/s.

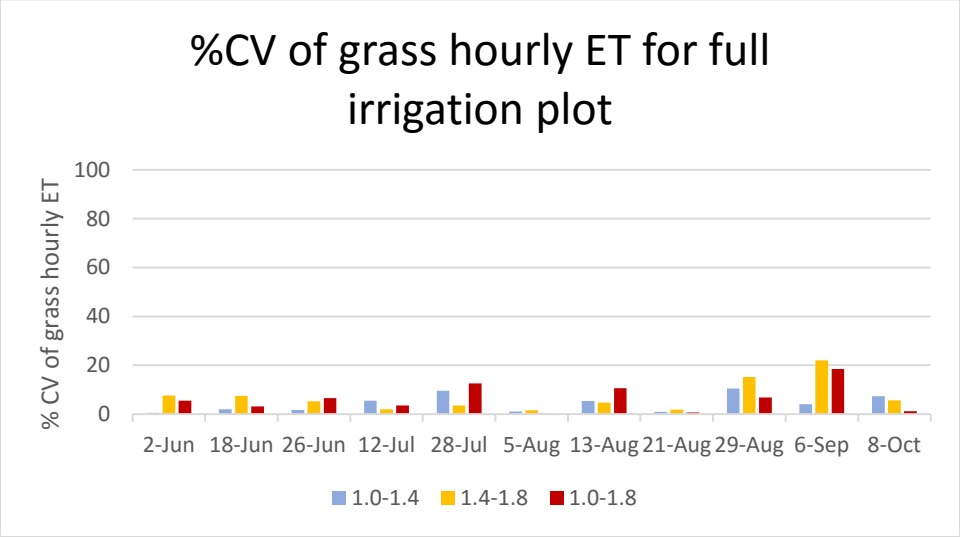

Figure 8 Clustered bar graph showing %CV of grass hourly ET for full irrigation treatment plot

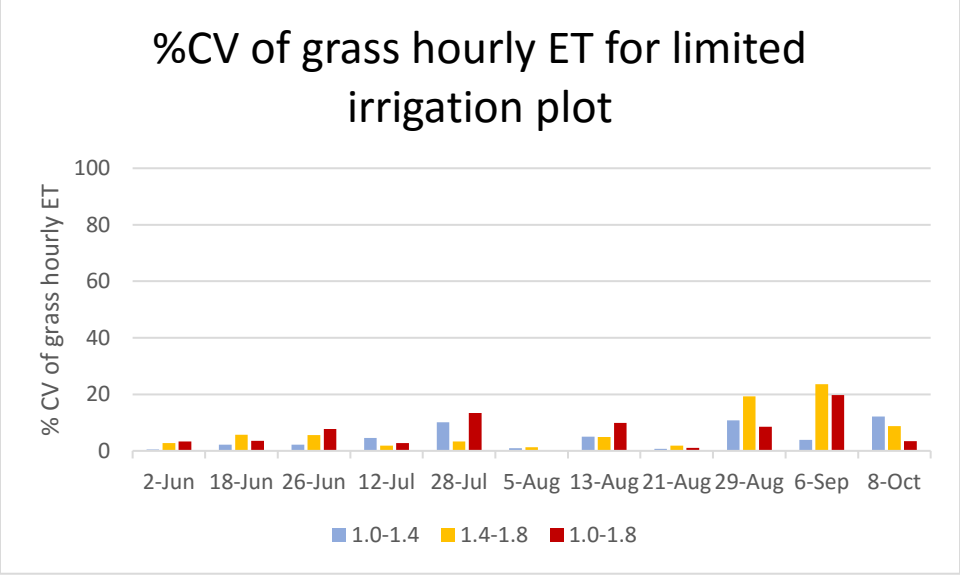

Figure 9 Clustered bar graph showing %CV of grass hourly ET for limited irrigation treatment plot

Since the 1-1.8 m/s cluster has a higher range (range is 0.8), the variability of grass hourly ET between these two wind speed assumptions is high, as expected. For this cluster, on average, the percent variability of grass ET is 6.3% (maximum of 12.6%) for full treatment plot and 6.7% (maximum of 19.7%) for the limited treatment plot. The least variability of grass ET is seen between 1 and 1.4 m/s (range is 0.4) - on average, 4.4% (maximum of 10%) for full treatment plot and 4.8% (maximum of 11%) for limited treatment plot. For 1.4 to 1.8 m/s (range is 0.4), the variability of grass ET is 6.9% (maximum of 22%) for full treatment plot and 7.2% (maximum of 23.5%) for limited treatment plot. This indicates that as the value of wind speed assumption increases, the variability of grass ET increases even though the range (0.4) is constant between 1-1.4 and 1.4-1.8 clusters. The %CVs for all the 3 ranges described is comparable for the two treatment plots. Overall, the %CV of grass hourly ET is approximately 6% on average, and thus the grass ET is not highly sensitive to wind speed values in or below the range tested.

3.1.3 ReSET evaluation

3.1.3.1 Evaluation with ground instruments

Daily ReSET-derived grass ET compared against ET estimated from the suite of ground instruments, that is, LAS, net radiometer and ground plates installed (hereafter called LAS-estimated) at the limited irrigation treatment plot for 7 overlapping satellite overpass dates in 2015 and 2016 is shown in Table 3.

Table 3 Comparison between daily LAS-estimated and ReSET-derived ET

Dates	LAS-estimated	ReSET-derived	% Difference
August 5, 2015	6.8	6.51	4.3
August 13, 2015	7.4	4.34	41.3

August 21, 2015	3.9	4.1	-5.1
August 29, 2015	5.2	4.1	21.2
June 4, 2016	6.5	4.6	29.2
June 20, 2016	6.3	4.7	25.4
July 14, 2016	4.2	1.8	57.1
			Average = 24.8

On average, the difference between the daily LAS-estimated and ReSET- derived ET was 24.8% on a daily basis, with a maximum difference of 57.1%. While the above data are from limited treatment plot, this plot was not stressed until the start of July of 2016, even though some stress-carryover from 2015 is possible. The above dataset was thus divided into stressed (August 5,13,21,29 in 2015 and July 14 in 2016) and non-stressed (June 4 and 20 in 2016) categories. It was estimated that the average difference for the former category is 23.8% and for the latter is 27.3%. Overall, it was observed that ReSET-derived ET is lower, and may point to some underestimation for both stressed and non-stressed categories. Figure 10 shows the LAS-estimated and ReSET-derived ET comparison with alfalfa reference ET from weather station (WS). It was observed that on August 13, 2015 (stressed category), LAS-estimated ET was higher than the reference ET (which is the maximum weather demand at any time period). Since this was the stressed category, the limited plot was not irrigated and according to the nearest COAGMET weather station (Montrose), negligible precipitation was received over the area in the past 3-4 days. Since the actual ET cannot be higher than the weather demand, this highlights the fact that these instruments may not be free of their own errors and limitations, and may not be considered as an absolute benchmark for evaluation. Another possibility could be a negative

sensible heat flux (sensible heat flux absorbed by the crops), which would cause an increase in available energy and thus an increase in actual ET.

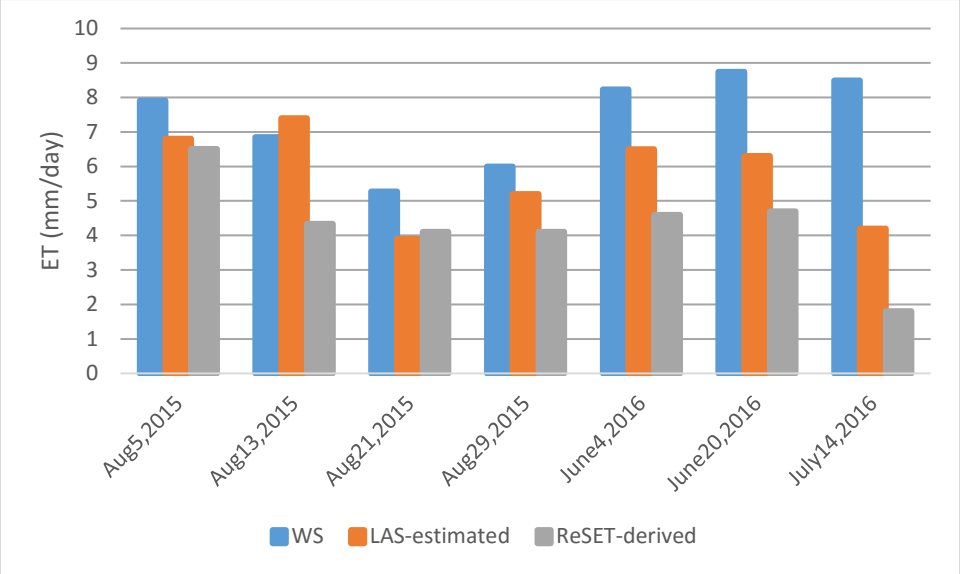

Figure 10 ET comparison between reference Weather Station (WS), LAS-estimated and ReSET-derived

3.1.3.2 Scene evaluation

Path 35/ Row 33

Scenes chosen at the time of peak alfalfa growth were June 2, 2015 and June 4, 2016, since the cutting after first crop growth cycle were observed to happen around/after the first week of June (as seen later in section 3.2. In 2016, for ground-verified alfalfa fields in the area, the maximum value of alfalfa crop coefficient obtained was 0.96. Since, the number of fields verified for crop type on ground was limited for the purpose (only 9 fields in the entire scene), the crop cover layer was also utilized to choose maximum values of alfalfa crop coefficients. Even though the crop cover layer was observed to be not entirely accurate because some alfalfa fields were classified as corn and some grass pastures as alfalfa, but corn fields were not classified as alfalfa- which means that choosing alfalfa layer was acceptable for this process because the maximum value of crop coefficients for alfalfa-classified fields would belong to alfalfa. The three most

highly transpiring, stress-free fields, after filtering, were selected from the crop cover layer, and combining their maximum crop coefficients with 0.96 (the maximum value of crop coefficient for ground-verified alfalfa) revealed the average maximum crop coefficient in the peak growth to be 0.98. Similarly, for 2015, the average maximum alfalfa crop coefficient was 1.04. This perhaps points to slight underestimation of ET in 2016 and slight overestimation in 2016 because crop coefficient in peak growth stage should ideally be 1. But crop coefficients at peak stage can be slightly lower or higher than 1 because of a slight difference of actual surface resistance, albedo etc. than assumed in FAO-56 Penman-Monteith equation. Overall, ReSET performed well in this peak growth season scene evaluation. It should be mentioned that this evaluation is only for peak period, and may vary during different crop growth stages and stress conditions.

Path 34/ Row 33

Scenes chosen for this overpass were July 7, 2016 and June 27, 2015. Since the area under this scene does not have alfalfa, the scene evaluation for maximum crop coefficient was done for grass pastures, and the aforementioned dates were selected on the basis of common knowledge of peak growth of grass pastures before their first cutting in mid-July (Dr. Perry Cabot, personal communication). The maximum crop coefficient of grass pastures after passing all the filtering checks was found to be 1.15 in 2016 and 1.1 in 2015. These crop coefficients of grass pastures are with respect to the reference alfalfa ET (ETr) because the physiology of these pastures is closer to alfalfa reference crop than short grass reference crop (ETo). Clearly, ReSET overestimated ET for the peak growth season of grass in this scene evaluation, perhaps due to excess water decreasing thermal signature leading to an increase in derived ET. Another issue could be selection of anchor pixels, especially cold pixels due to all the small/narrow water bodies which can erroneously lead to selection of a colder cold pixel- which has high NDVI and is highly transpiring due to sufficient water availability. This would lead to an underestimation of

ET, if selection of hot pixel is correct and is not affected by saline/mineralated soils. To further explore the selection of cold and hot pixels in this complex scene, the overlapping area between this Path34/Row33 and Path35/Row33 was compared. The reasoning was that since crop coefficients estimated over a given area (overlapping area between two images) do not change significantly over a day, crop coefficients determined over Gunnison and Uncompahgre imagery on consecutive overpass days can be compared for evaluating the estimation of ET over Gunnison area, and to check the anchor points' selection in Path34/Row33 imagery. Figure 11 shows the difference of average crop coefficients from the two overpass scenes (Path34/Row33 – Path35/Row33) over the entire growing season- one image per month (except September when no cloud-free subsequent images existed) to capture the overall trends, with data from 2015 complementing 2016 when needed. Assuming that the ET estimation for Path35/Row33 is accurate and not affected by hot and/or cold pixel miscalibration, it was observed that in peak growth, selection of hot and cold pixels may not be an issue because the average difference of crop coefficient between the two is minimal in June (peak of first growth cycle) and August (peak after crop regrows after first cutting). But, there is underestimation in July and October that could be due to selection of a colder cold pixel, and overestimation in May could be due to selection of a hotter hot pixel since selection of a right hot pixel is relatively more important in the beginning of season because of faster heating up of soils with salt or minerals in them. In such a situation, an energy balance model that is not based on anchor pixels, like Two-Source model, may perform better and is worth evaluating in future research.

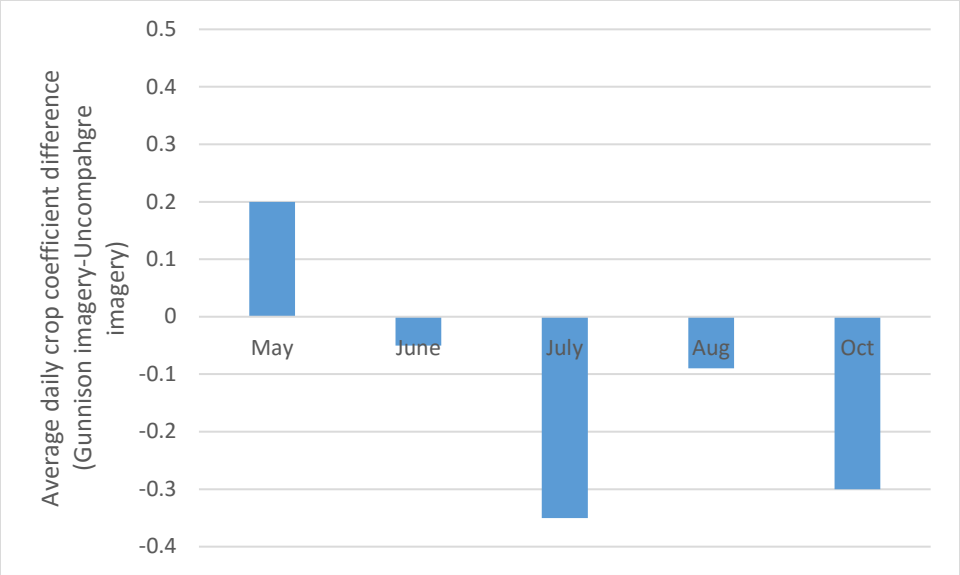

Figure 11 Average daily crop coefficient difference, calculated from consecutive overpass days

3.1.4 Conserved CU (CCU)

Monthly CCU calculated for 2015 (August-October) and 2016 (April-July) for Montrose site as a result of ET difference at full and limited irrigation plots is shown in figure 12. CCU increased gradually from August to October in 2015 after the limited plot was stressed in August. There was some stress carryover in 2016 on the limited plot because ET or CU on this plot is not as high in April and May of 2016, even though this plot was not stressed during this time period. June CCU is slightly negative which could be an artifact of slightly higher irrigation on limited irrigation plot around the satellite overpass dates in June. July CCU is again positive, which is expected since the limited plot was stressed in this month.

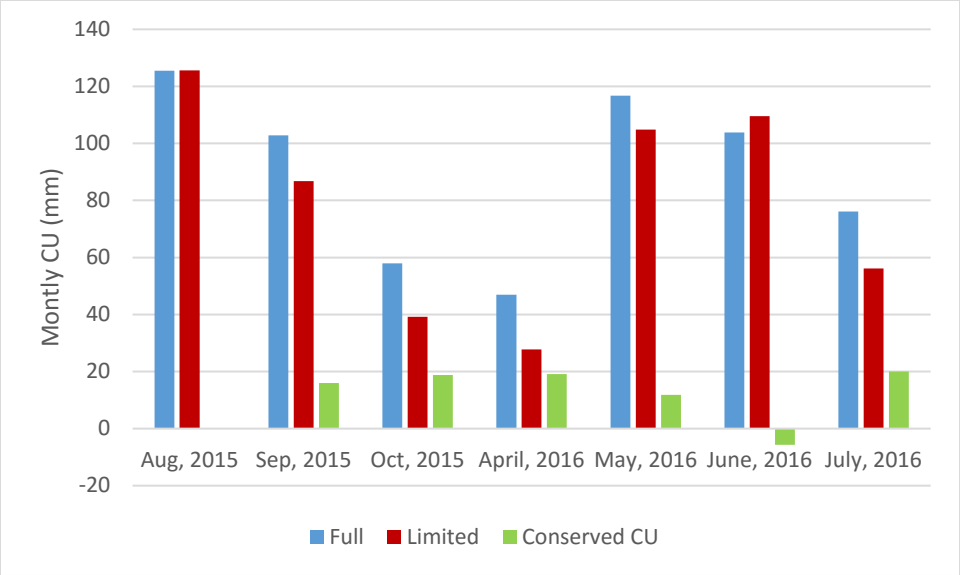

Figure 12 Monthly Full, Limited and Conserved CU (mm/month)

3.1.5 Number of cloud-free images

As noted from 2015-2016 data, for both Uncompahgre and Gunnison overpasses, the number of cloud-free images was found to be adequate in the middle of the growing season- from June to August, with an average of 2-3 cloud-free images per month. The month of April usually has 1 cloud-free image for the Uncompahgre overpass, but none for the higher elevation Gunnison overpass. The months of May, September and October have 1-2 cloud-free images for Uncompahgre overpass and 0-1 for Gunnison overpass. According to Allen et al. (2015) and Elhaddad et al. (2011), a minimum of one image per month is necessary for season estimates of CU. For monthly estimates, more than one imagery per month may often be necessary, especially for these pasture crops which go through different cutting cycles and rapidly changing phenology over a month. For tracking crop changes better, utilizing other satellites with thermal band (like MODIS Aqua/Terra which has 1 km thermal band) conjunctively with Landsat after utilizing pixel sharpening technique (Agam et al., 2007) to run ReSET model, or utilizing a different approach like reflectance-based crop coefficient method (that does not require a thermal

band) with satellites like Sentinel in conjunction with Landsat to increase temporal frequency, can be considered in the future.

3.2 Local growth stage lengths

3.2.1 Grass

To avoid any classification error in crop cover layer, average NDVI of 16 ground-truthed grass pasture fields were tracked through the beginning of March to the beginning of September (a total of 21 cloud-free images) with Sentinel 2 MSI, Landsat 7 and 8 to estimate local growth stage lengths of each cutting cycle because NDVI is directly related to crop coefficients (Without Sentinel, the number of cloud-free images for this time period were only 13). After filtering, 10 fields were chosen. Three out of these 10 fields showed 3 cutting cycles until the beginning of September, which probably meant that these fields were a mix, with some alfalfa in them- even though their NDVI was not as high as alfalfa (alfalfa fields tend to have a NDVI >0.8 at peak stage; as in figure in 13). These fields were excluded for this analysis- but do highlight the complexity of water management due to highly variable agronomic practices in the area. The average NDVI for the remaining fields, with 2 cutting cycles until the beginning of September, is shown in figure 13. According to FAO-56, the growing season for grass pastures can be estimated to begin 7 days before the last -4 ˚C in spring. Following this FAO-56 guideline, the growing season can be estimated to begin on March 30 in 2016. The lengths of grass growth stages mentioned in FAO-56 are 10 and 20 days for initial and development growth stages respectively for the first cutting cycle. No information is provided for the rest of the cutting cycles.

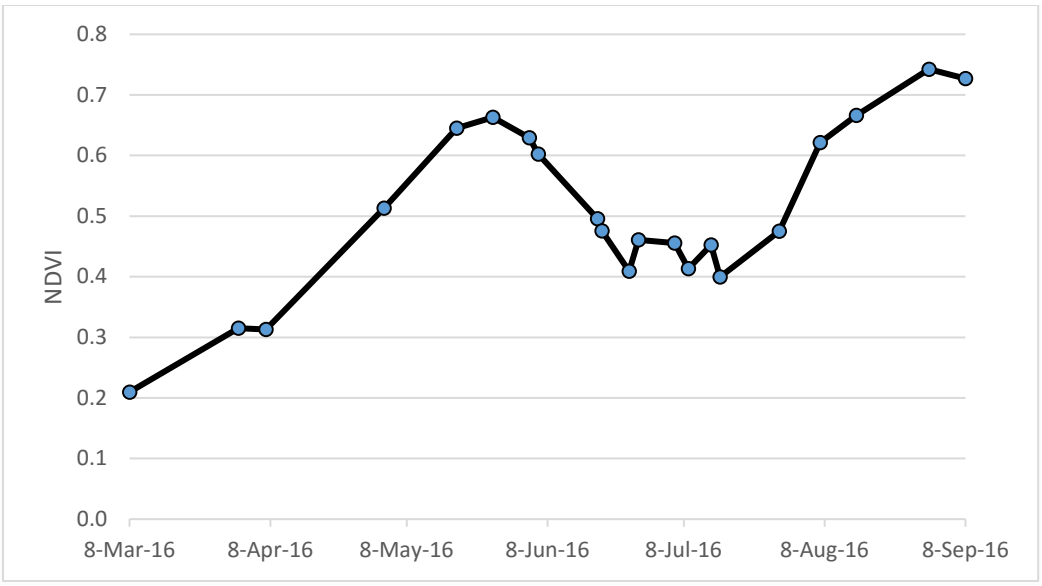

Figure 13 Grass pastures crop growth (related to NDVI) with time

Values of NDVI increased from March 8 to April 1, which shows a green-up of perennial grass pastures. This was followed by the initial stage with nearly constant NDVI for about 7 days, which is similar to FAO-56 value of 10 days for initial stage. The development stage for the first cutting cycle lasted for 42 days, which is twice as long as mentioned in FAO-56(20 days). This could be because of the elevation differences between the Uncompahgre and Idaho (University of Idaho Agricultural Experiment Station, Moscow, Idaho). The high elevation of the Uncompahgre causing cooling of air could be one reason for the delay of crop growth. The mid and late season lasted for a total of 37 days. It is unclear if the second cutting cycle has an initial growth stage due to slight noise perhaps due to atmospheric or sensor differences from June 28-July 16. The second development stage lasted 45 days, while FAO-56 does not provide any information about the growth stage lengths after the first cutting cycle. It is also noted that this information maybe specific to the limited number of ground-truthed and filtered fields used, and additional analysis on more number of fields and for more number of years needs to be done in the future.

3.2.2 Alfalfa

Similar to grass pastures, average NDVI of 9 ground-truthed alfalfa pasture fields were tracked through March to September with the same 3 satellites, and filtering process resulted in 4 desirable fields which were used to construct the average NDVI curve shown in Figure 14. It was observed that there were 3 cutting cycles of alfalfa until the beginning of September. According to FAO-56, the growing season for alfalfa can be estimated to begin on the day the last -4 ˚C temperature happened in spring, which was on April 6 in 2016. The lengths of alfalfa growth stages mentioned in FAO-56 for Idaho, USA, are 10, 30, 25, and 10 days for initial, development, mid and late growth stages respectively for the first cutting cycle; and 5, 20, and 10 days for initial, development, mid and late growth stages respectively for all other cutting cycles.

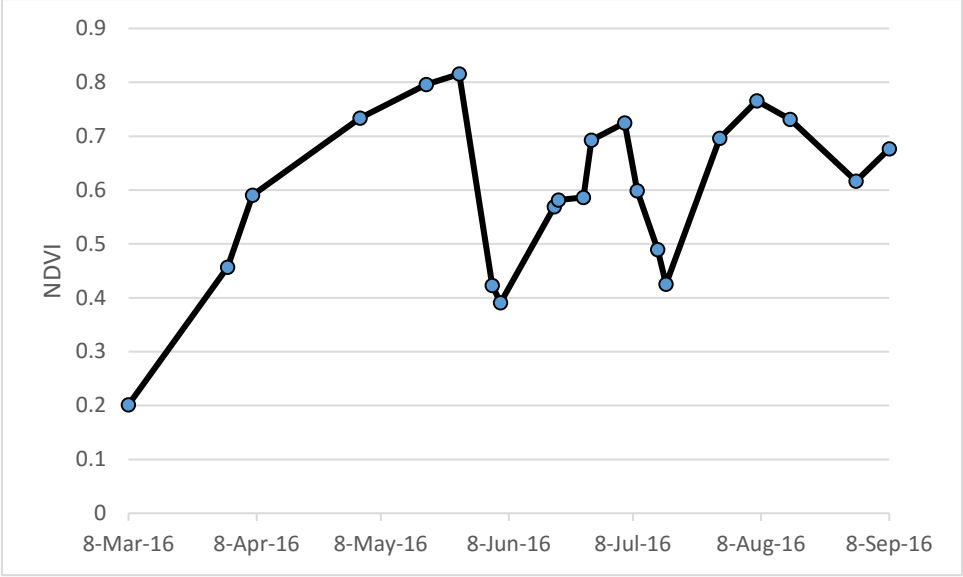

Figure 14 Alfalfa pastures crop growth (related to NDVI) with time

The crop growing season starts from April 6 (last -4 ˚C), but from figure 14, it was observed that from March 8 to April 7, NDVI increased gradually perhaps referring to the perennial crop green-up period. Initial growth stage was not seen for any cutting (for the first cutting cycle as well as subsequent cycles, right after each cutting). This could be due to rapid crop development

after the crop green-up before the first cycle, and for other cycles – perhaps the crop does not need that initial stage since it is already an established crop. Another reason could be that the crops were not cut all the way down their entire height – in such a case, an initial growth stage is not needed. The number of days, for the development stage at the first cycle, on average was found to be 42; which is equivalent to number of days for FAO-56 initial (10) and development (30) stages. For the second and third cutting cycles, the number of days in each period was 22 and 21, respectively, which is equivalent to FAO-56(20). Mid and late growth stage lengths are highly variable, depending on farmers' condition and decision which is related to factors like size of the field (e.g., if the size of field is very big, cutting will take several days), grazing patterns (e.g.., animals maybe let out for grazing as soon as the crops reach peak growth for all or one/more than one of the cutting cycles; how many animals graze a field, how long animals are let out in the field for grazing) etc. The average number of days, for mid and late stages combined, were found to be 18, 18, and 24 for first, second and third cutting cycles, which is roughly similar to FAO-56 (35, 20, and 20). It is also noted that this information maybe specific to the limited number of ground-truthed and filtered fields used, and additional analysis on more number of fields and for more number of years needs to be done in the future.

3.3 Reflectance-based empirical model for grass pastures

The filtered fields in section 3.2.1 were utilized to generate an empirical model between Kc and NDVI. The scatter plot obtained between ReSET-derived Kc's and NDVI is shown in figure 15 and the linear equation for line-of-best fit is:

$$Kc = 1.195\ NDVI - 0.057 \quad (R^2 = 0.72) \qquad (3.1)$$

This is an empirical regression model that can be utilized with reflectance-based crop coefficient approach. Since this model is developed from ReSET, it inherently contains the errors of ReSET

(perhaps due to low wind speed or atmospheric lapse rate correction), if any. The model has a NSCE of 0.71, MBE of -0.05% and RMSE of 20%. Since it was difficult to determine surface conditions (dry or wet) of fields used in model formulation, the Kc used here is a single crop coefficient- which is the sum of basal crop coefficient (Kcb), and the contribution of soil evaporation (Ke). Since different surface condition are considered together, the magnitude of variance (or RMSE) about the best line of fit is also relatively high. The model may be improved in the future using known surface conditions (perhaps utilizing an index like Normalized Difference Moisture Index that is sensitive to wet/moisture conditions)– but in that case, when applying the specific-surface conditions model (e.g., Kcb for conditions where soil is not wet and evaporation is low), the surface condition of the fields should be known too. The model derived here in its current form can be utilized to calculate near-real time ET without the need of thermal band, perhaps with other multispectral satellites like Sentinel 2 MSI to increase the temporal resolution.

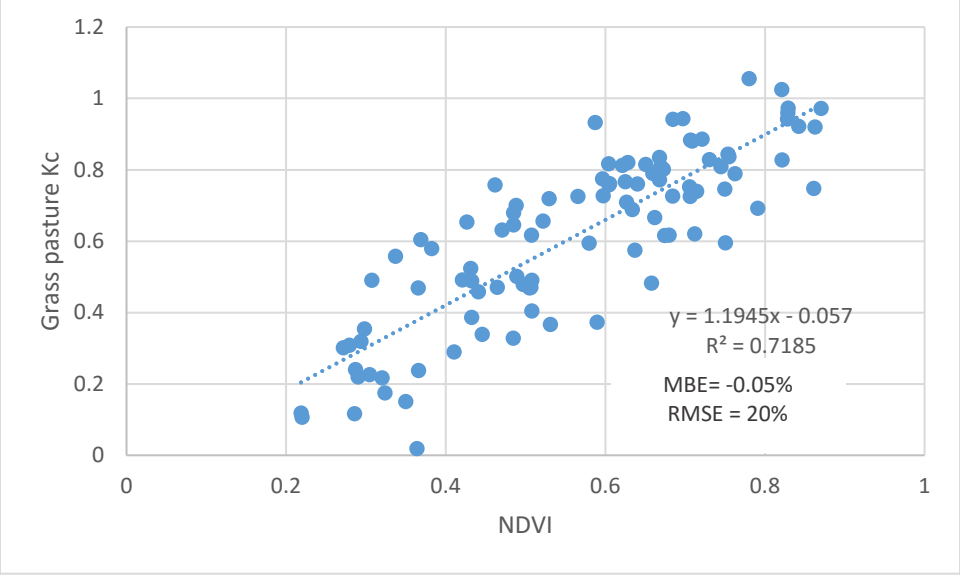

Figure 15 Scatter plot between Kc and NDVI

3.4 Evaluation of reflectance-based empirical models

3.4.1 Grass pastures

Reflectance-based empirical model developed in section 3.3 was applied to both full and limited plots at Montrose site, which is approximately 5 km away from a weather station. After obtaining the reflectance-based crop coefficient from (3.1), the alfalfa reference ET (ETr) from weather station was multiplied with it to determine actual ET. Table 4 shows the performance of this approach on daily average basis with respect to Reset-derived daily ET. The model performed better for the full irrigation plot (average MBE and RMSE of 0.64 and 1.02 mm/day, respectively; NSCE of 0.63) than at the limited plot (average MBE and RMSE of 0.69 and 1.09 mm/day, respectively; NSCE of 0.52) because short-term stresses may not affect the NDVI, but affects the ET rates. Overall, the performance of this method for grass pastures is similar to ReSET on a daily basis and has a potential to be utilized with a combination of several multispectral satellites to get a higher temporal resolution ET product in almost near-real time.

Table 4 Grass pastures: Error analysis of Reflectance-based daily ET with respect to ReSET-derived daily ET

	Full irrigation field	Limited irrigation field
MBE (mm/day)	0.64	0.69
MBE (%)	13	21
RMSE (mm/day)	1.02	1.09
RMSE (%)	15	23
NSCE	0.63	0.52

3.4.2 Alfalfa pastures

Singh and Irmak (2009) alfalfa-based empirical model derived in Nebraska was evaluated with respect to ReSET outputs at 3 alfalfa sites approximately 5 km away from weather stations for 2015 and 2016. Table 5 summarizes the MBE, RMSE and NSCE of the daily ET outputs of this method with respect to ReSET-derived daily ET. The performance of this method for alfalfa is similar to ReSET and has a potential to be utilized with a combination of several multispectral satellites to get a higher temporal resolution ET product in almost near-real time. The errors observed from alfalfa model were slightly lower than that for locally-developed grass model- this was attributed to the higher number of alfalfa fields used in Singh and Irmak (2009) than used in this study.

Table 5 Alfalfa pastures: Error analysis of Reflectance-based daily ET with respect to ReSET-derived daily ET

MBE (mm/day)	0.16
MBE (%)	3
RMSE (mm/day)	1.13
RMSE (%)	22
NSCE	0.60

CHAPTER 4: CONCLUSIONS AND RECOMMENDATIONS

This study performed a preliminary evaluation of ReSET model for agro-climatological conditions of the Western Slope. Wind sensitivity analysis revealed that grass hourly ET was not very sensitive to wind speed, especially at lower values. Evaluation of grass daily ET with ground sensors pointed to an underestimation by about 25%. But it was also noted that the ground instruments had their own limitations. Besides, as has been noted in previous studies, these errors may decrease on an average for a longer time period, like monthly. A scene based evaluation of grass ET was also done for peak growth stage and it was observed that the ReSET model performed well for the Uncompahgre. Overall, this preliminary evaluation reveals a high potential of ReSET to be utilized in the Uncompahgre for the estimation of daily CU at large spatial scales for alternate water transfer methods like water banks.

It is recommended that further evaluation of ReSET under both full and limited irrigation conditions on a monthly time- scale, which is practically more appropriate for an operation water bank needs to be carried out. Although CCU estimated showed expected trends due to recession of irrigation, further validation needs to be done using lysimeter or neutron probe ET estimation.

The selection of anchor pixels for calibrating the Gunnison imagery was questionable due to complex agro-hydrological area. For geographically complex Gunnison area, future research should explore other energy-based models like Two Source model which do not rely on anchor pixels. But nonetheless, the plethora of narrow water bodies, and type of irrigation (flood) in the Gunnison area may reduce the thermal signature of canopy in the image, and may present a

challenge to any remote sensing based methodology. For Gunnison area, a conclusive evaluation is thus needed to determine the use of remote sensing methodologies in reliable quantification of CU for water sharing arrangements.

Crop growth stages' lengths were tracked with Landsat and Sentinel satellites, and provide important information regarding local growth stage lengths for grass and alfalfa pastures in the area. A NDVI-Kc relationship for grass pastures was also developed. This relationship was evaluated for energy and water limiting conditions on grass, and results showed that it performed similar to ReSET daily estimates. Errors were higher for stressed crop because NDVI does not capture short-term/immediate stresses. Previously developed Nebraska-based NDVI-Kc relationship for alfalfa was also evaluated, and it also performed similar to daily ReSET estimates. The errors observed from alfalfa model were slightly lower than that for locally-developed grass model; this was attributed to the higher number of alfalfa fields used in the Nebraska-based study than used in this study.

The NDVI-Kc approach can be a promising tool for estimating near-real time ET in the future for water sharing arrangements, especially when utilized with a combination of Landsat 7, Landsat 8, Sentinel 2a MSI and Sentinel 2b MSI(to be launched in 2017) satellites. The monthly CU (and subsequently CCU) estimation using this approach on an enhanced temporal scale has a potential to overcome the limitations of using the energy balance approach which relies on the thermal bands - thus a limited temporal frequency of only Landsat satellites.

REFERENCES

Agam, N., Kustas, W. P., Anderson, M. C., Li, F., & Neale, C. M. (2007). A vegetation index based technique for spatial sharpening of thermal imagery. *Remote Sensing of Environment*, *107*(4), 545-558.

Allen, R. G., Pereira, L. S., Raes, D., & Smith, M. (1998). Crop evapotranspiration-Guidelines for computing crop water requirements-FAO Irrigation and drainage paper 56. *FAO, Rome*, *300*(9), D05109.

Allen, R.G. (2002) RefET: Reference evapotranspiration calculator. Version 2.01.17, *Utah State University Foundation, Logan.*

Allen, R.G., Tasumi M., & Morse A. (2005). Satellite-based evapotranspiration by METRIC and Landsat for western states water management. *US Bureau of Reclamation Evapotranspiration Workshop, Feb 8–10, 2005, Ft. Collins*.

Allen, R. G., Tasumi, M., & Trezza, R. (2007a). Satellite-based energy balance for mapping evapotranspiration with internalized calibration (METRIC)—Model. *Journal of irrigation and drainage engineering*, *133*(4), 380-394.

Allen, R. G., Tasumi, M., Morse, A., Trezza, R., Wright, J. L., Bastiaanssen, W., ... & Robison, C. W. (2007b). Satellite-based energy balance for mapping evapotranspiration with internalized calibration (METRIC)—Applications.*Journal of irrigation and drainage engineering*, *133*(4), 395-406.

Allen, R., Irmak, A., Trezza, R., Hendrickx, J. M., Bastiaanssen, W., & Kjaersgaard, J. (2011). Satellite-based ET estimation in agriculture using SEBAL and METRIC. *Hydrological Processes*, *25*(26), 4011-4027.

Ambast, S. K., Keshari, A. K., & Gosain, A. K. (2002). Satellite remote sensing to support management of irrigation systems: concepts and approaches. *Irrigation and drainage*, *51*(1), 25-39.

ASCE-EWRI (2005). The ASCE standardized reference evapotranspiration equation. *In: Allen RG, Walter IA, Elliot RL, et al. (eds.) Environmental and Water Resources Institute (EWRI) of the American Society of Civil. Engineers, ASCE, Standardization of Reference Evapotranspiration Task Committee Final Report,213pp. Reston, VA: American Society of Civil Engineers (ASCE).*

Barnett, T. P., Pierce, D. W., Hidalgo, H. G., Bonfils, C., Santer, B. D., Das, T., ... & Cayan, D. R. (2008). Human-induced changes in the hydrology of the western United States. *Science*, *319*(5866), 1080-1083.

Bastiaanssen, W. G. M., Menenti, M., Feddes, R. A., & Holtslag, A. A. M. (1998). A remote sensing surface energy balance algorithm for land (SEBAL). 1. Formulation. *Journal of hydrology*, *212*, 198-212.

Bausch, W. C. (1995). Remote sensing of crop coefficients for improving the irrigation scheduling of corn. *Agricultural Water Management*, *27*(1), 55-68.

Best, A. (2009) Tapped Out. *Published online: http://lawweb.colorado.edu/law/centers/nrlc/events/documents/oil%20shale/Tapped%20Out%20by%20Alan%20Best%20%20(October%20'09).pdf Accessed 06/06/2016.*

Brutsaert, W., & Sugita, M. (1992). Application of self-preservation in the diurnal evolution of the surface energy budget to determine daily evaporation. *Journal of Geophysical Research: Atmospheres*, *97*(D17), 18377-18382.

Brutsaert, W., Hsu, A. Y., & Schmugge, T. J. (1993). Parameterization of surface heat fluxes above forest with satellite thermal sensing and boundary-layer soundings. *Journal of Applied Meteorology, 32*(5), 909-917.

Budyko, M. I. (1961). The heat balance of the earth's surface. *Soviet Geography*, *2*(4), 3-13.

CDM. (2011). Colorado's Water Supply Future. Final Report. *Submitted to Colorado Water Conservation Board. May 2011*.

Chen, A., Abramson, A., Becker, N., & Megdal, S. B. (2015). A tale of two rivers: pathways for improving water management in the Jordan and Colorado River Basins. *Journal of Arid Environments, 112*, 109-123.

Colby, B., Jones, L., & O'Donnell, M. (2014). Supply reliability under climate change: Forbearance agreements and measurement of water conserved. In*Water markets for the 21st century* (pp. 57-82). Springer Netherlands.

Cook, J., & Rabotyagov, S. S. (2014). Assessing irrigators' preferences for water market lease attributes with a stated preferences approach. *Water Resources and Economics, 7*, 19-38.

CWCB (Colorado Water Conservation Board). (2007). Statewide Water Supply Initiative-Phase 2. *Final Report, Section 3- Alternative Agricultural Water Transfer Methods to Traditional Purchase and Transfer*. *November 2007. Prepared by Camp Dresser & McKee Inc.*

Deering, D. W. (1978). Rangeland reflectance characteristics measured by aircraft and spacecraft sensors. *Ph.D. Diss. Texas A&M Univ., College Station*, 338p

Doherty, T., Smith, R., Schempp,A., Alylward,B. (2012). Water transfers in the West. Projects, Trends, and Leading Practices in Voluntary Water Trading.

Elhaddad, A., & Garcia, L. A. (2008). Surface energy balance-based model for estimating evapotranspiration taking into account spatial variability in weather. *Journal of irrigation and drainage engineering*, *134*(6), 681-689.

Elhaddad, A., & Garcia, L. A. (2011). ReSET-raster: surface energy balance model for calculating evapotranspiration using a raster approach. *Journal of Irrigation and Drainage Engineering*, *137*(4), 203-210.

Elhaddad, A., Garcia, L. A., & Chávez, J. L. (2010). Using a surface energy balance model to calculate spatially distributed actual evapotranspiration. *Journal of irrigation and drainage engineering*, *137*(1), 17-26.

Er-Raki, S., Chehbouni, A., Guemouria, N., Duchemin, B., Ezzahar, J., & Hadria, R. (2007). Combining FAO-56 model and ground-based remote sensing to estimate water consumptions of wheat crops in a semi-arid region. *Agricultural water management*, *87*(1), 41-54.

Fereres, E., & Soriano, M. A. (2007). Deficit irrigation for reducing agricultural water use. *Journal of experimental botany*, *58*(2), 147-159.

Fritschen, L. J., & Bavel, C. V. (1962). Energy balance components of evaporating surfaces in arid lands. *Journal of Geophysical Research*, *67*(13), 5179-5185.

GAO. (2005). "KLAMATH RIVER BASIN Reclamation Met Its Water Bank Obligations, but Information Provided to Water Bank Stakeholders Could Be Improved." *Reports to Congressional Requesters No. 05-283, Government Accountability Office, www.gao.gov/cgibin/getrpt?GAO-05-283, March.*

Gentine, P., Entekhabi, D., & Polcher, J. (2011). The diurnal behavior of evaporative fraction in the soil-vegetation-atmospheric boundary layer continuum. *Journal of Hydrometeorology*, *12*(6), 1530-1546.

Gitelson, A. A., & Merzlyak, M. N. (1996). Signature analysis of leaf reflectance spectra: algorithm development for remote sensing of chlorophyll. *Journal of plant physiology*, *148*(3), 494-500.

Gowda, P. H., Chavez, J. L., Colaizzi, P. D., Evett, S. R., Howell, T. A., & Tolk, J. A. (2008). ET mapping for agricultural water management: present status and challenges. *Irrigation science*, *26*(3), 223-237.

Hunsaker, D. J., Pinter Jr, P. J., Barnes, E. M., & Kimball, B. A. (2003). Estimating cotton evapotranspiration crop coefficients with a multispectral vegetation index. *Irrigation Science*, *22*(2), 95-104.

Hutson, S. S. (2004). *Estimated use of water in the United States in 2000*(No. 1268). Geological Survey (USGS).

Irmak, A., Kamble, B., Ratcliffe, I., Kjaersgaard, J., Huntington, J., Trezza, R., & Allen, R. G. (2012). *Operational remote sensing of ET and challenges*. INTECH Open Access Publisher.

Jackson, R. D. (1984, October). Remote sensing of vegetation characteristics for farm management. In *1984 Technical Symposium East* (pp. 81-97). International Society for Optics and Photonics.

Jayanthi, H., Neale, C. M., & Wright, J. L. (2007). Development and validation of canopy reflectance-based crop coefficient for potato.*Agricultural water management*, *88*(1), 235-246.

Jones, Lana, and Bonnie G. Colby. "Measuring, Monitoring, and Enforcing Temporary Water Transfers: Considerations, Case Examples, Innovations and Costs." *Innovative Water Transfer Tools for Regional Adaptation to Climate Change* (2012).

Kalma, J. D., McVicar, T. R., & McCabe, M. F. (2008). Estimating land surface evaporation: A review of methods using remotely sensed surface temperature data. *Surveys in Geophysics, 29*(4-5), 421-469.

Keplinger, K. O., McCarl, B. A., Chen, C. C., & Ward, R. (1998). *The 1997 irrigation suspension program for the Edwards Aquifer: Evaluation and alternatives*. Texas Water Resources Institute, The Texas A & M University System.

Libecap, G. D. (2010). Water rights and markets in the US semi arid west: efficiency and equity issues.

MacDonald, G. M. (2010). Water, climate change, and sustainability in the southwest. *Proceedings of the National Academy of Sciences, 107*(50), 21256-21262.

McIntire, M. V. (1970). Disparity between State Water Rights Records and Actual Water Use Patterns-I Wonder Where the Water Went, The. *Land & Water L. Rev., 5*, 23.

McNaughton, K. G., & Black, T. A. (1973). A study of evapotranspiration from a Douglas fir forest using the energy balance approach. *Water Resources Research, 9*(6), 1579-1590.

Meijninger, W. M. L. (2003). Surface fluxes over natural landscapes using scintillometry. *PhD Thesis, Wageningen University, 2003.*

Michael, M (1978): Irrigation theory and Practices: Vikas Publishing House. pp 546-548; 584-681; 709-722

Mkhwanazi, M., Chávez, J. L., & Andales, A. A. (2015a). SEBAL-A: A remote sensing ET algorithm that accounts for advection with limited data. Part I: Development and validation. *Remote Sensing, 7*(11), 15046-15067.

Mkhwanazi, M., Chávez, J. L., Andales, A. A., & DeJonge, K. (2015b). SEBAL-A: A remote sensing ET algorithm that accounts for advection with limited data. Part II: Test for transferability. *Remote Sensing*, *7*(11), 15068-15081.

MWH. 2012. Colorado River water bank feasibility study- Phase 1. MWH Americas, Inc.

Neale, C. M., Bausch, W. C., & Heermann, D. F. (1990). Development of reflectance-based crop coefficients for corn. *Transactions of the ASAE*,*32*(6), 1891-1900.

Neale, C. M., Jayanthi, H., & Wright, J. L. (2003, September). Crop and irrigation water management using high resolution airborne remote sensing. In *Proceedings of 54th IEC meeting of the international commission on irrigation and drainage (ICID) workshop remote sensing of ET for large regions* (Vol. 17).

Norviel, W. S., W. F. McClure, D. E. Carpenter, J. G. Scrugham, S. B. Davis, R. E. Caldwell, and F. C. Emerson. 1922. *Colorado River Compact, 1922. Santa Fe, NM, USA.*

Peters, N. E., & Meybeck, M. (2000). Water quality degradation effects on freshwater availability: impacts of human activities. *Water International*,*25*(2), 185-193.

Qualls, R. J., & Brutsaert, W. (1996). Effect of vegetation density on the parameterization of scalar roughness to estimate spatially distributed sensible heat fluxes. *Water Resources Research*, *32*(3), 645-652.

Qualls, R., & Hopson, T. (1998). Combined use of vegetation density, friction velocity, and solar elevation to parameterize the scalar roughness for sensible heat. *Journal of the atmospheric sciences*, *55*(7), 1198-1208.

Ray, S. S., & Dadhwal, V. K. (2001). Estimation of crop evapotranspiration of irrigation command area using remote sensing and GIS. *Agricultural water management*, *49*(3), 239-249.

Rock, B. N., Vogelmann, J. E., Williams, D. L., Vogelmann, A. F., & Hoshizaki, T. (1986). Remote detection of forest damage. *BioScience*, *36*(7), 439-445.

Singh, R. K., & Irmak, A. (2009). Estimation of crop coefficients using satellite remote sensing. *Journal of irrigation and drainage engineering*,*135*(5), 597-608.

Solomon, S. (Ed.). (2007). *Climate change 2007-the physical science basis: Working group I contribution to the fourth assessment report of the IPCC* (Vol. 4). Cambridge University Press.

Taghvaeian, S. (2011). Water and energy balance of a riparian and agricultural ecosystem along the Lower Colorado River. *Ph.D. Diss. Utah State University, 2011*.

Tasumi, M. (2003). Progress in operational estimation of regional evapotranspiration using satellite imagery. *Ph.D. Diss. University of Idaho, 2003.*

Taylor, S. A., Ashcroft, G. L., Brady, N. C., Baver, L. D., Gardner, W. R., Brady, N. C., & Weil, R. R. (1972). Physical edaphology: the physics of irrigated and nonirrigated soils (No. 631.43 T246). *Centro Regional de Ayuda Técnica, México, DF (México).*

Trezza, R. (2002). Evapotranspiration using a satellite-based surface energy balance with standardized ground control. *Ph.D. Diss. Utah State University, 2002.*

USBR. (2012). Colorado River Basin Water Supply and Demand Study. In *AGU Fall Meeting Abstracts* (Vol. 1, p. 1362).

USGS. (2005). Assessment of the Klamath Project Pilot Water Bank: A Review from a Hydrologic Perspective. *Portland: United States Geological Survey*.

Vano, J. A., Udall, B., Cayan, D. R., Overpeck, J. T., Brekke, L. D., Das, T., ... & Morino, K. (2014). Understanding uncertainties in future Colorado River streamflow. *Bulletin of the American Meteorological Society*, *95*(1), 59-78.

Young, M. D. (2010). Environmental Effectiveness and Economic Efficiency of Water Use in Agriculture. *OECD Studies on Water*, 1-33.

APPENDICES

Appendix 1

Table 6 COAGMET Weather Stations

S.NO.	Weather Station Name	Elevation(m)
1	Montrose	1722
2	Delta	1527
3	Eckert	1683
4	CSU Fruita Exp. Station	1378
5	CSU Rogers Mesa Exp Station	1691
6	Orchard Mesa	1402
7	Olathe 1	1623
8	Olathe 2	1662
9	Gunnison	2406

Appendix 2

ReSET model

1. Hourly alfalfa reference ET was first computed from the weather station data (comprising of temperature, relative humidity, vapor pressure, wind speed and solar radiation) using RefET software (Allen, 2002).
2. Daily alfalfa reference ET was calculated by summing up the hourly ET values.
3. Spatially interpolated reference ET (hourly and daily) and wind speed from all the weather stations was created using the Inverse Distance Weight (IDW) function.
4. After calculating reflectance and brightness temperature (T_b) Landsat bands, surface radiometric temperature (Ts) was calculated by:

$$Ts = \frac{T_b}{\varepsilon_{NB}^{0.25}}$$

Where ε_{NB} is barrow bans surface emissivity = 0.97 +0.0033 LAI. LAI is the Leaf area index. If LAI is >3, this value is set equal to 0.98.

5. The surface radiometric temperature was then corrected using atmospheric lapse rate correction, as seen in equation (2.1).
6. Net radiation flux (Rn) was determined by:

$$Rn = R_{s\downarrow} - \alpha R_{s\downarrow} + R_{L\downarrow} - R_{L\uparrow} - (1 - e_o)R_{L\downarrow}$$

Where $R_{s\downarrow}$ is incoming short-wave radiation (W m^{-2}), α is surface albedo (dimensionless), $R_{L\downarrow}$ is incoming long-wave radiation (W m^{-2}), $R_{L\uparrow}$is outgoing long-wave radiation (W m^{-2}) and e_o is broadband surface thermal emissivity.

7. Ground heat flux was determined by the following equation:

$$\frac{G}{R_n} = 0.005 + 0.18E^{-0.521LAI} \quad (LAI \geq 0.5)$$

$$\frac{G}{R_n} = \frac{1.80(T_s - 273.15)}{R_n} + 0.084 \quad \text{(LAI <0.5)}$$

8. Sensible heat flux was given by

$$H = \frac{\rho C_p dT}{r_{ah}}$$

where dT is the near surface temperature difference(K); ρ is the air density (kg/m^3), Cp is the specific heat of air (1004 J/kg/K), and r_{ah} is the aerodynamic resistance to heat transport(s/ m)

9. The near surface temperature difference (dT) is assumed to be linearly related with Ts

dT = a Ts +b

This linear equation has two unknowns thus needs two conditions to be solved. This is where the concept of hot and cold pixels comes in. In ReSET, more than once hot and cold pixels are selected, and then an interpolation between them produces hot and cold rasters, such that the above equation is solved for every pixel.

10. The aerodynamic resistance to heat transport (r_{ah}) was given by

$$r_{ah} = \frac{\ln(\frac{z_2}{z_1})}{u*k}$$

where z_1 and z_2 are near surface levels, 0.1 and 2 m respectively, k is von karman constant equal to 0.4, and u* is friction velocity

11. The friction velocity (u*) was given by

$$u* = \frac{ku_x}{\ln(\frac{z_x}{z_{om}})}$$

Where u_x is wind sped (m/s) at height z_x above the ground, and z_{om} is the momentum roughness length (m)

12. The momentum roughness length (z_{om}) was calculated as a function of LAI

$$z_{om} = 0.018 \text{ LAI}$$

A minimum value of 0.005 is set for z_{om} when LAI tends to zero.

13. The LAI was derived as a function of Soil Adjusted Vegetation Index (SAVI)

$$LAI = -\frac{\ln(\frac{0.69-SAVI}{0.59})}{0.91}$$

14. Initially, the sensible heat flux was calculated assuming neutral atmospheric conditions. Atmospheric stability corrections were done using the Monin-Obukhov (M-O) Similarity Theory (MOST). The M-O length (L) was calculated using the following equation:

$$L = -\frac{\rho C_p u*^3 T_s}{kgH}$$

where g is gravitational constant. If L>0, the atmosphere is stable; if L=0, the atmosphere is neutral, if L<0, atmosphere is unstable. The stability iterations were repeated until the H stabilizes (change in H between two consecutive iterations in <5%)

15. Then, the latent heat flux (LE) was computed as a residual of the energy balance:

$LE = R_n - G - H$

16. Instantaneous(hourly) ET was then computed from the LE

$$ET_{inst} = 3600 \frac{LE}{\lambda \rho_w}$$

where ρ_w is 1,000 kg/m^3, and λ is given by $(2.501 - 0.00236(T_{air} - 273.15)). 10^6$ (J/kg)

17. Reference ET fraction (ETrF) was then computed by dividing the E_{inst} by spatially interpolated hourly reference ET raster

$$ETrF = \frac{ET\_inst}{ET_r}$$

18. Daily ET(ET_d) was then calculated by using the ETrF function as follows:

$$ET_d = ETrF \text{ X } ET_{r\_d}$$

Where ETr_d is the spatially interpolated reference daily reference ET raster from the weather stations

LAS description and calculations

The LAS operates by transmitting a near-infrared (880 nm) electromagnetic beam between a transmitter and receiver, which is affected by "scintillations" or turbulence in the beam path caused by variations in the air refractive index (*n*) (Meijninger, 2003). The receiver captures the strength of the transmitted signal and correspondingly accounts for the variation of the signal strength in time. The LAS was installed at limited irrigation plot at a height of approximately 2.17 m, and the distance between the transmitter and receiver being 192 m. The relationship between the measured variance of the natural logarithm of intensity fluctuations (σ_{lnI}^2) and the structure parameter of the air refractive index (C_n^2 , $m^{-2/3}$) exists:

$$C_n^2 = 1.12\sigma_{lnI}^2 D^{7/3} L^{-3} \quad (1)$$

where D is the aperture diameter, L is the distance between transmitter and receiver (path length).

Cn^2 can be decomposed into the structure parameters of temperature, and humidity. For NIR wavelengths, temperature fluctuations (C_T^2, K. $m^{-2/3}$) are the main contributors to Cn^2.

$$C_T^2 = \frac{T^2}{A_T^2} \cdot \frac{C_n^2}{(1+\frac{0.03}{B})^2} \quad (2)$$

where B is bowen ratio (H/LE), $A_T = -0.78.10^{-6}\frac{B_p}{T}+0.126.10^{-6} R_v q$ and T is air temperature (K), BP is barometric pressure, R_v is water vapor gas constant and q is specific humidity. Subsequent application of Monin-Obukhov (M-O) similarity theory (MOST) permits the determination of the temperature scale (T*, K).

$$T* = \left(\frac{C_T^2 (z_{LAS}-d)^{\frac{2}{3}}}{f_T(\frac{z_{LAS}-d}{L_{mo}})} \right)^{0.5} \quad (3)$$

z_{LAS} is the effective LAS beam height (m), d is the zero displacement height (m), and f_T represents the MOST similarity function for CT^2 and T*. In order to determine H, additional input of the friction velocity (u*, m s^{-1}) is required.

$$u* = \frac{k_v.(u2-u1)}{\ln\left(\frac{(z_2-d)}{(z1-d)}\right)-\psi\left(\frac{z_2-d}{L_{mo}}\right)+\psi\left(\frac{z_1-d}{L_{mo}}\right)} \quad (4)$$

The equation for u* above represents the logarithmic wind profile model, where k_v is the Von Karman constant (~0.41), U represents horizontal wind speed (m s^{-1}) at two heights, z1 and z2 (m), and ψ represents the M-O similarity functions for u*. Both T* and u* are dependent (in a thermally stratified surface layer) on similarity functions of the buoyancy parameter (z/L_{mo}), where z (m) represents the measurement height less the zero displacement height (d, m) and L_{mo} is the Monin-Obukhov length (m). The computations are different for unstable and stable atmospheric conditions; independent determination of the atmospheric stability condition was made from ancillary data from two thermometers installed vertically at the study site. Both T* and u* are dependent (in a thermally stratified surface layer) on similarity functions of the buoyancy parameter (z/L_{mo}), where z (m) represents the measurement height less the zero displacement height (d, m) and L_{mo} is the Monin-Obukhov length (m). L_{mo} is also dependent on T* and u*, thus requiring an iterative computation to obtain H from Cn^2 measurement.

$$H = -\rho_{air} c_p u* T* \quad (5)$$

where is ρ_{air} density of air and c_p is the specific heat of dry air at constant pressure (~ 1,005 J. Kg^{-1}. K^{-1}).